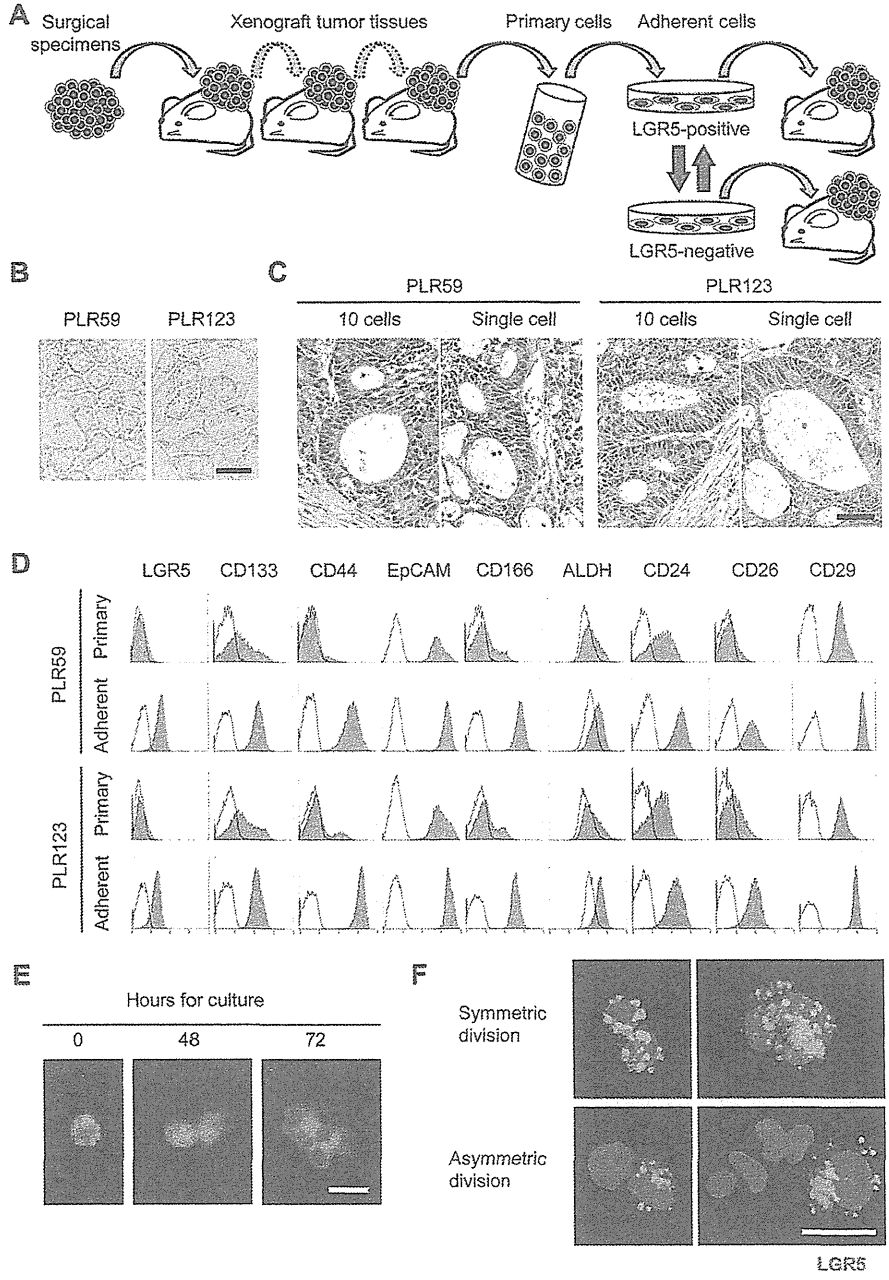

Figure 2. Characteristics of colon cancer cell lines with cancer stem cell (CSC) properties. **(A):** Schematic representation of the process for the establishment of colon cancer cell lines. **(B):** Phase contrast microscopy of the cells in the LGR5$^+$ cell lines. Cells were collected from xenografts of PLR59 and PLR123 after more than 10 passages in NOD/Shi-*scid*. IL-2Rγ^{null} (NOG) mice and cultured under an adherent culture condition. Bar = 20 μm. **(C):** Histology of the tumors derived from the LGR5$^+$ cells from PLR59 and PLR123 xenografts. Ten or single LGR5$^+$ cells from the adherent cultures of the cells derived from PLR59 and PLR123 xenografts were subcutaneously injected into NOG mice. Bar = 50 μm. **(D):** Expression of CSC markers. The primary cells from xenografts of PLR59 and PLR123 after more than 10 passages in NOG mice (upper) and the LGR5$^+$ cells cultured under an adherent culture condition (lower) were analyzed by flow cytometry. Shadow, Fluorescent intensities after staining with the indicated antibodies or ALDH activity; Open, Fluorescent intensities after staining with control isotype antibody or ALDH activity with an ALDH inhibitor. **(E):** Symmetric division of the LGR5$^+$ cells. The LGR5$^+$ cells stained with PKH67 dye were cultured for 72 hours and examined by fluorescent microscopy. Bar = 20 μm. **(F):** Symmetrical (upper) and asymmetrical (lower) divisions of the LGR5$^+$ cells in the presence or absence of Matrigel and fetal bovine serum. Photographs of the cells were taken after single division (left) and after two or three divisions (right). The LGR5$^+$ cells were cultured for 48–72 hours and stained with the anti-LGR5 antibody. Bar = 20 μm.

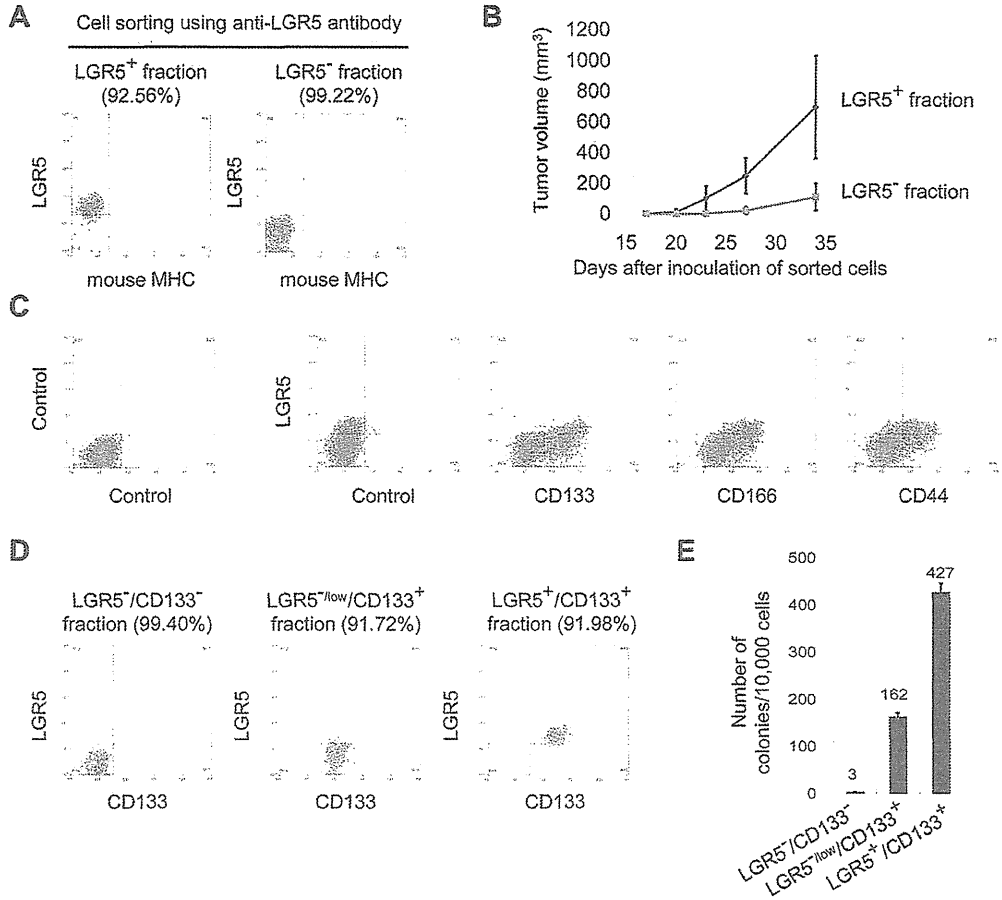

Figure 3. Colony forming activity and tumorigenicity of the sorted LGR5$^+$ and the LGR5$^-$ cells. **(A):** Flow cytometry analysis of the sorted LGR5$^+$ and LGR5$^-$ populations from the primary cells of PLR123 xenograft generated by the inoculation of the LGR5$^+$ cells. Percentages indicate the purity of the sorted cell population. **(B):** Tumor formation by the sorted LGR5$^+$ and the LGR5$^-$ cells. One thousand cells of the sorted LGR5$^+$ and the LGR5$^-$ populations suspended in Matrigel were subcutaneously inoculated into NOG mice, and tumor volume was measured. Mean ± SD of six tumors is shown. **(C):** Flow cytometry analysis of the primary cells from the PLR123 xenograft after staining with anti-LGR5 antibody together with anti-CD133, anti-CD166, or anti-CD44 antibody. **(D):** Flow cytometry analysis of the cells in the sorted LGR5$^-$/CD133$^-$, LGR5$^{-/low}$/CD133$^+$ and LGR5$^+$/CD133$^+$ populations from the primary cells of the PLR123 xenograft. Percentages indicate the purity of the sorted cell population. **(E):** Colony forming activity of the sorted LGR5$^-$/CD133$^-$, LGR5$^{-/low}$/CD133$^+$ and LGR5$^+$/CD133$^+$ cells. Ten thousand cells of the sorted cells were seeded on Matrigel. Number of colonies after culturing the cells for 6 days was determined. Mean ± SD in triplicate experiments is shown.

Interconversion Between LGR5$^+$ Proliferating and LGR5$^-$ Drug-Resistant States

We next asked whether the LGR5$^+$ cells exhibited a drug-resistant state, which is believed to be a typical characteristic of CSCs [37]. After treatment of the LGR5$^+$ cells with irinotecan for 3 days, the cells stopped proliferation and about half of the cells survived (Supporting Information Fig. S5). One hundred percent of the surviving cells became LGR5$^-$, but they retained other colon CSC markers (Fig. 4A, 4B; Supporting Information Fig. S6, Table S4). The LGR5$^-$ cells induced by treating the LGR5$^+$ cells with an anticancer drug were designated as drug-resistant LGR5$^-$ cells in this study. LGR5$^-$ cells which were pre-existing in xenograft tissues and human tumor tissues are referred to as LGR5$^-$ cells. Reverse transcriptase real-time polymerase chain reaction (RT-qPCR) for *LGR5*, *CD133*, *CD44*, *CD166*, and *EPCAM* revealed that the *LGR5* mRNA was drastically decreased after irinotecan treatment, but the mRNAs of *CD133*, *CD44*, *CD166*, and *EPCAM* did not decline or even increased after treatment (Supporting Information Fig. S7D). The mRNA level of *CK20* did not increase by the irinotecan treatment and remained at a low level (Supporting Information Fig. S2A). Although we cannot rule out the possibility that elimination of epitope by proteolytic cleavage on LGR5 occurred after irinotecan treatment, the cells that were not recognized by any of our anti-LGR5 antibodies were regarded as LGR5 negative. We examined the TIA of these drug-resistant LGR5$^-$ cells. Even injection of the 10 LGR5$^-$ cells formed tumors in two sites (PLR59-derived cells), and the PLR123-derived cells formed tumors at one site out of six injection sites in the NOG mice (Supporting Information Table S5). Treatment of the LGR5$^+$ cells with 5-fluorouracil or oxaliplatin also gave rise to drug-resistant LGR5$^-$ cells which converted to an LGR5$^+$ state after re-seeding and culturing in the absence of the drugs (Supporting Information Fig. S8).

The drug-resistant LGR5$^-$ cells did not grow even after irinotecan was removed from the culture medium

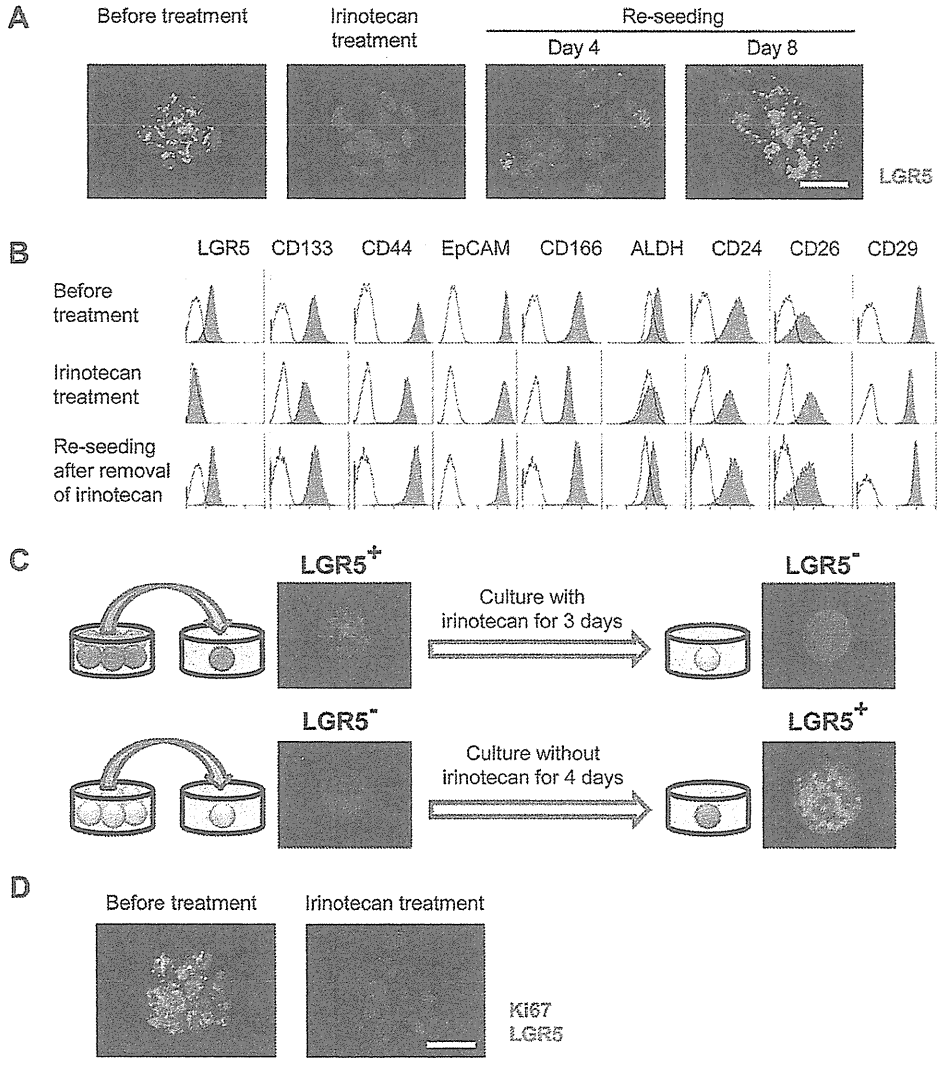

Figure 4. Transition of the colon cancer stem cells (CSCs) between $LGR5^+$ and $LGR5^-$ states in vitro. **(A):** Immunostaining of LGR5 after treatment of the $LGR5^+$ cells with irinotecan. The adherent $LGR5^+$ cells from PLR123 xenografts cultured in the presence of irinotecan became $LGR5^-$. The drug-resistant $LGR5^-$ cells were re-seeded and further cultured in the absence of irinotecan for the indicated days. The $LGR5^+$ cells appeared 4 days after the reseeding and increased by 8 days. Bar = 50 μm. **(B):** Expression of CSC markers. The $LGR5^+$ cells from the adherent cultures from PLR123 xenografts before (top) and after treatment with irinotecan (middle) were analyzed by flow cytometry. Cells re-seeded after irinotecan treatment (bottom) were also analyzed. Shadow, Fluorescent intensities after staining with the indicated antibodies or ALDH activity; Open, Fluorescent intensities after staining with control isotype antibody or ALDH activity with an ALDH inhibitor. **(C):** Interconversion of the $LGR5^+$ and $LGR5^-$ states in vitro. $LGR5^+$ cells collected by flow cytometry were seeded by limiting dilutions and cultured under an adherent culture condition in the presence of irinotecan for 3 days. Drug-resistant $LGR5^-$ cells that had been treated with irinotecan were seeded by limiting dilutions and cultured under an adherent culture condition for 4 days. The cells were stained with anti-LGR5 antibody to confirm the expression of LGR5. LGR5 was visualized by R-phycoerythrin (PE)-labeled anti-mouse IgG (red) or by AlexaFluor 488-labeled anti-mouse IgG (green). **(D):** Ki67 staining of the $LGR5^+$ and drug-resistant $LGR5^-$ cells. In vitro cultures of the $LGR5^+$ cells and the drug-resistant $LGR5^-$ cells obtained by the treatment of the adherent $LGR5^+$ cells with irinotecan were double stained with the anti-LGR5 antibody and an anti-Ki67 antibody. Bar = 50 μm.

(Supporting Information Fig. S5C). However, they became positive for LGR5 and resumed proliferation after replating (Fig. 4A, 4B). The transition from the $LGR5^+$ state to an $LGR5^-$ state and vice versa was also confirmed by observations with single cells in culture. When single $LGR5^+$ cells were cultured in multiwell plates, the cells transitioned to an $LGR5^-$ state within 3 days after irinotecan treatment. When single $LGR5^-$ cells that had been treated with irinotecan were then cultured in multiwell plates without irinotecan, 19%–43% of the cells converted to the $LGR5^+$ state within 4 days (Fig. 4C; Supporting Information Table S6). In order to confirm proliferation of the $LGR5^+$ and drug-resistant $LGR5^-$ cells, we also used double staining of LGR5 and Ki67 with the in vitro cultures of the $LGR5^+$ and the $LGR5^-$ cells. The expression of LGR5 correlated well with Ki67 staining: the $LGR5^+$ cells were positive for Ki67, and the drug-resistant $LGR5^-$ cells were negative for Ki67 (Fig. 4D).

Pathway analysis using the results of DNA microarray of both proliferating LGR5$^+$ and drug-resistant LGR5$^-$ cells revealed characteristics of two distinct states. As expected from the growth status of the cells, genes involved in cell cycle were downregulated whereas genes in the p53 signaling pathway were upregulated in the drug-resistant LGR5$^-$ cells (Supporting Information Fig. S9). Genes whose mRNA expression increased in the LGR5$^!$ cells included those involved in cell growth such as *LGR5*, *FGFBP1*, *FGFR4*, *RORI*, *NFIA*, *PIGU*, *LPAR3*, and *FZD2* (Supporting Information Fig. S7C).

Reconstitution of the Epithelial Cell Type Tumor Hierarchy from LGR5$^+$ Cells

The observations that the cells converted from the LGR5$^+$ to the drug-resistant LGR5$^-$ state in vitro and that the drug-resistant LGR5$^-$ cells formed tumors in vivo prompted us to examine whether the drug-resistant LGR5$^-$ cells directly generate a tumor hierarchy of differentiated cell types or first convert to the LGR5$^+$ state in vivo. To detect drug-resistant LGR5$^-$ cells, we attempted to identify the genes that are upregulated in the drug-resistant LGR5$^-$ cells by comparing the gene expression profiles of the drug-resistant LGR5$^-$ cells, the LGR5$^+$ cells, and the primary cells from the xenografts. From the gene expression analyses of DNA microarray, a heat map is shown (Fig. 5A; Supporting Information Fig. S7) for the top 20 genes encoding membrane proteins with the largest change. Genes whose mRNA expression was increased in the drug-resistant LGR5$^-$ cells include MHC class II-related genes (*HLA-DMA*, *HLA-DMB*), adhesion molecule-related genes (*AMIGO2*, *FLRT3*, *GJB5*, *CLDN1*), G-protein-coupled receptor protein signaling pathway-related genes (*GPR87*, *GPR110*, *GPR172B*, *GNAI1*, *ABCA1*), and immune signaling-related genes (*TNFSF15*, *BLNK*, *FAS*, *TMEM173*). We further evaluated the genes for which antibodies against their proteins are available (Supporting Information Table S7).

Immunohistochemical staining of the cells cultured in vitro with antibodies confirmed that HLA-DMA was rather specifically expressed in the drug-resistant LGR5$^-$ cells (Fig. 5B). HLA-DMA was located in intracellular vesicles, and therefore, it cannot be used for cell sorting. Nevertheless, HLA-DMA can be a useful molecule for identifying the LGR5$^-$ cells in xenografts and in clinical specimens. Because HLA-DMA is also expressed in macrophages, we looked for genes that were expressed in both LGR5$^!$ and drug-resistant LGR5$^-$ cells and identified EREG (Fig. 5A). Immunohistochemical staining with a monoclonal antibody against EREG confirmed the EREG expression in LGR5$^+$ and LGR5$^-$ cells (Fig. 5B; Supporting Information Fig. S10). By combination of these markers, LGR5$^-$ cells can be detected as HLA-DMA and EREG double positive cells. After injection of a homogenous population of drug-resistant LGR5$^-$ cells into NOG mice, cells weakly expressing LGR5 but still positive for HLA-DMA and EREG appeared within 1 day after the injection, and then the LGR5$^+$/EREG$^+$ cells which were negative for HLA-DMA emerged by day 5 (Fig. 5C). The reconstitution of the epithelial tumor hierarchy of diverse cell types from the drug-resistant LGR5$^-$ cells through transition to LGR5$^!$ cells was confirmed (Fig. 5D).

We next examined the possibility of a conversion of LGR5$^!$ cells to a drug-resistant state in vivo. NOG mice bearing tumors derived from the LGR5$^!$ cells were administered intraperitoneally with a maximum tolerated dose (MTD) dose (120 mg/kg) of irinotecan. Tumor growth was nearly completely inhibited (Fig. 5E), and ductal structures were heavily destroyed (Fig. 5F). Under such conditions, the LGR5$^+$ cells were markedly decreased (Fig. 5F; Supporting Information Fig. S11). There was a significant increase in HLA-DMA-positive cells, which are LGR5$^-$, after irinotecan treatment. In contrast, about one-third of the cancer cells in both ducts and budding regions were LGR5$^+$ in the vehicle-treated control mice. Both LGR5$^!$ cells and HLA-DMA$^!$/LGR5$^-$ cells were positive for EREG (Fig. 5F). The LGR5$^!$ cells reappeared after termination of irinotecan treatment (Fig. 5F; Supporting Information Fig. S11). We also performed double staining with Ki67 and LGR5 or HLA-DMA that marks LGR5$^-$ CSCs. As in the in vitro cultured cells, there was a good correlation of LGR5 expression and Ki67 staining of the cells in the xenografts. The LGR5$^!$ cells were positive for Ki67, and the LGR5$^-$/HLA-DMA$^+$ cells were negative for Ki67 (Fig. 5G). Thus, tumor reconstitution occurred through the LGR5$^+$ cells.

Possible Therapeutic Application of Anti-EREG Antibody

EREG is expressed on the surface of both LGR5$^!$ and drug-resistant LGR5$^-$/HLA-DMA$^+$ cells, but its expression is very low or hardly detectable in differentiated tumor cells and normal tissues (Fig. 5A; Supporting Information Fig. S12A). Therefore, EREG may be a potential therapeutic target. We first examined the growth inhibitory activity and antibody dependent cell cytotoxicity (ADCC) activity of the anti-EREG antibody. The anti-EREG antibody induced ADCC activity against both LGR5$^+$ and drug-resistant LGR5$^-$ cells in the presence of human peripheral blood mononuclear cells (PBMC) that contained effector cells, such as natural killer (NK) cells and monocytes, but the antibody did not directly affect the growth of LGR5$^+$ and drug-resistant LGR5$^-$ cells in the absence of effector cells in vitro (Supporting Information Fig. S12B, S12C). To test the expression of EREG in vivo, we subcutaneously inoculated the LGR5$^+$ cells into NOG mice in which EREG was highly expressed during early stages of tumor development, and later its expression was rather restricted to budding areas as compared to ducts when tumors formed clear duct structures. EREG-positive cells were also detected after the mice bearing the tumors were administered irinotecan (Fig. 5F). Therefore, we tested the antitumor activity of the anti-EREG antibody after irinotecan treatment. SCID mice were used as a model for efficacy evaluation, because the antibody requires effector cells to elicit ADCC. When the antibody was administered at day 4 and day 11 after the final administration of irinotecan, it only delayed the tumor growth (Supporting Information Fig. S12D).

To test the efficacy in a metastatic model, we first examined the expression of EREG in metastasized tumors. When the LGR5$^!$ cells were intravenously injected into NOG mice, tumors were developed in several organs including the lung. For the tumors that developed in the lung, the majority of tumor cells were EREG positive (Fig. 6A). Efficacy was then tested using SCID-Beige mice in which macrophages and monocytes can serve as effectors for ADCC. When the antibody was administered once a week for five times starting 3 days after the tumor injection, the number of tumors at different sites was significantly decreased as compared to the control mice (Fig. 6B). In addition, the size of each tumor was also markedly reduced in the antibody treated mice (Fig. 6C, 6D).

The Existence of Both LGR5$^+$ and LGR5$^-$ Cells in Human Colon Cancers

We asked whether LGR5$^!$ and LGR5$^-$ cells could be detected in tissue sections of clinical colon cancers. Although rare, the LGR5$^!$ cells and the LGR5$^-$ cells which were HLA-DMA$^+$/EREG$^+$ were present in primary and metastatic colon cancer tissues from patients (Fig. 7A). Among 12 human

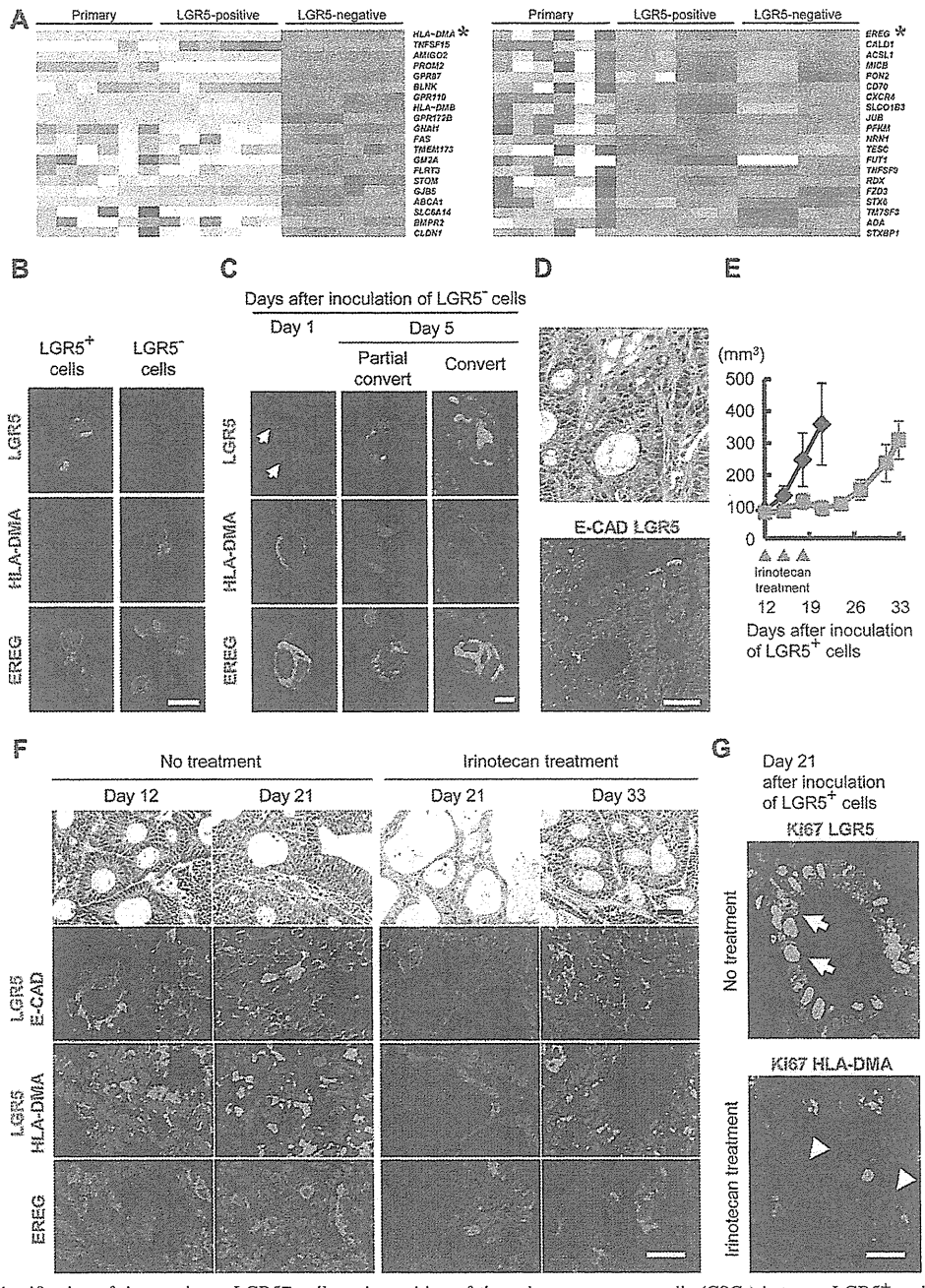

Figure 5. Identification of drug-resistant LGR5$^-$ cells and transition of the colon cancer stem cells (CSCs) between LGR5$^+$ and LGR5$^-$ states in vivo. **(A):** DNA microarray. RNA prepared from the primary cells from xenografts, LGR5$^+$ cells, and drug-resistant LGR5$^-$ cells derived from PLR59 and PLR123 were analyzed by Affymetrix U133. Heat map of 20 genes whose expression was markedly upregulated in the drug-resistant LGR5$^-$ cells as compared to the LGR5$^+$ cells (left) and that of 20 genes whose expression was increased in both LGR5$^+$ and drug-resistant LGR5$^-$ cells as compared to the primary cells from the xenografts (right) are shown. **(B):** Expression of HLA-DMA and EREG in LGR5$^+$ and drug-resistant LGR5$^-$ cells. The LGR5$^+$ (left) and drug-resistant LGR5$^-$ cells (right) derived from PLR123 xenografts were stained with anti-LGR5 antibody (top), anti-HLA-DMA antibody (middle), and anti-EREG antibody (bottom). Bar = 10 μm. **(C):** Transition from drug-resistant LGR5$^-$ cells to LGR5$^+$ cells during the early process of tumor development. The drug-resistant LGR5$^-$ cells derived from PLR123 xenografts were injected into NOG mice, and the tumors derived from the drug-resistant LGR5$^-$ cells were stained with anti-LGR5, anti-HLA-DMA, and anti-EREG antibodies. Arrow: Weakly staining of LGR5 on Day 1. Two typical types of cells are shown. Partial convert: Moderate staining of LGR5 with weakly staining of HLA-DMA on Day 5. Convert: Strong staining of LGR5 with no staining of HLA-DMA on Day 5. Bar = 10 μm. **(D):** Reconstitution of tumor hierarchy from the drug-resistant LGR5$^-$ cells. Histology (upper) and immunostaining with the anti-LGR5 and E-cadherin antibodies (lower) are shown. Bar = 50 μm. **(E):** Tumor volume of the xenografts. The LGR5$^+$ cells of PLR123 were subcutaneously injected into NOG mice, and the mice were administered irinotecan (120 mg/kg per day) 12, 15, and 18 days after the inoculation of the tumor cells. Tumor volume of the control mice (black line) and that of the mice which received irinotecan (red line) are shown. Each value represents mean ± SD (n = 5). **(F):** Histology and immunostaining for LGR5, HLA-DMA, and EREG of the tumors after treatment of irinotecan. Sections of the xenografts in (E) were excised from the mice at the indicated days after the inoculation of the LGR5$^+$ cells and stained with H&E, anti-LGR5 antibody, anti-HLA-DMA antibody, or anti-EREG antibody. Bar = 25 μm. **(G):** Ki67 staining of the LGR5$^+$ and the HLA-DMA$^+$ cells in xenografts. The sections of the xenografts excised from the mice 21 days after the inoculation of the LGR5$^+$ cells with or without treatment of irinotecan were double stained with anti-Ki67 antibody and anti-LGR5 antibody or anti-HLA-DMA antibody. Arrows: LGR5$^+$/Ki67$^+$ cells, arrow heads: HLA-DMA$^+$/Ki67$^-$ cells. Bar = 25 μm. Abbreviation: EREG, epiregulin.

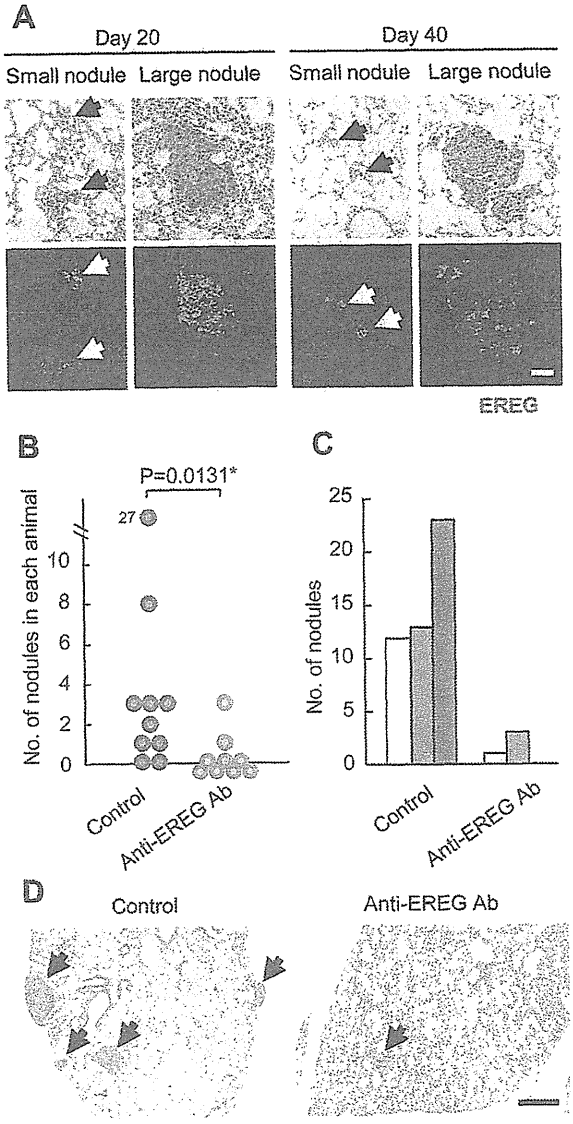

Figure 6. Antitumor activity of anti-EREG antibody. **(A):** Histology (upper) and immunostaining for EREG (lower) of the tumors. The adherent LGR5$^+$ cells derived from PLR123 xenografts were intravenously injected into NOD/Shi-*scid*, IL-2Rγ^{null} (NOG) mice. Tumors were dissected on the indicated days after inoculation of tumor cells. Photographs of typical large and small nodules are shown. Bar = 50 μm. **(B–D):** Numbers and histology of tumors in lung. Severe combined immunodeficiency (SCID)-Beige mice were intravenously injected with the adherent LGR5$^+$ cells derived from PLR123 xenografts. The anti-EREG antibody was administered every week for five times starting from 3 days after the tumor inoculation. Lung of the animals were resected and examined histologically with 11 cross-sections of the lung per animal (n = 10 for control group and n = 9 for anti-EREG antibody injected group). Number of tumor nodules per animal is shown in (B). Each symbol represents individual animal. Total numbers of tumor nodules in each group of the mice with the indicated sizes are shown in (C). Yellow column: under 100 μm, green column; 100–200 μm, red column; over 200 μm. Histology of the tumors with or without administration of anti-EREG antibody are shown in (D). Bar = 200 μm. Abbreviation: EREG, epiregulin.

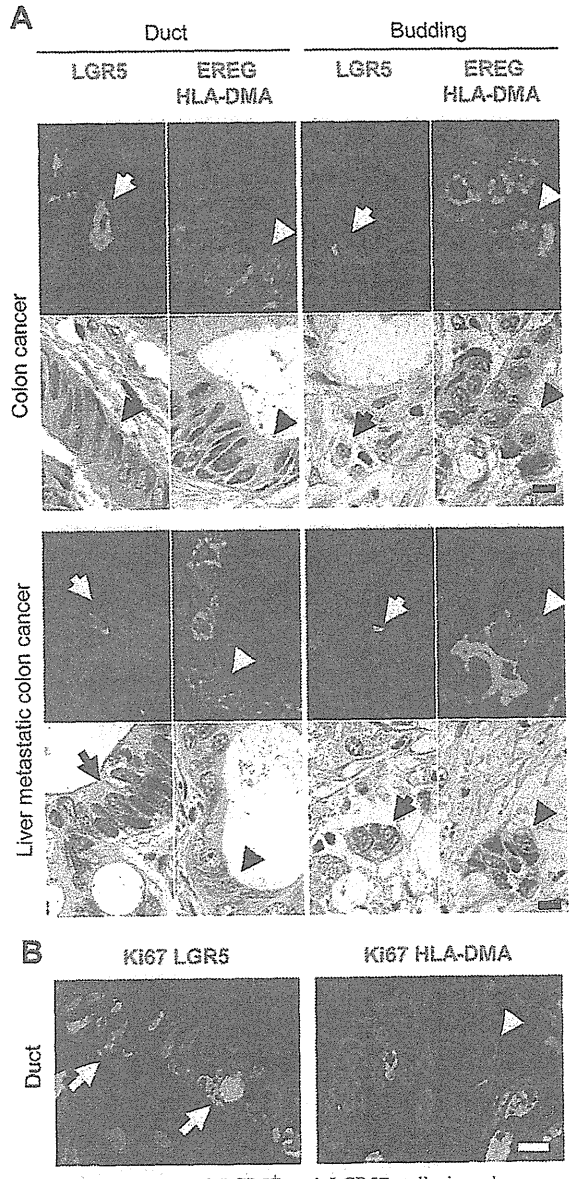

Figure 7. Presence of LGR5$^+$ and LGR5$^-$ cells in colon cancer and liver metastatic colon cancer from patients. **(A):** The same section of the primary and liver metastatic colon cancer tissues from patients was stained with H&E or antibodies against LGR5, HLA-DMA, and EREG. LGR5$^+$ and EREG$^+$/HLA-DMA$^+$ cells are detected in both ductal structures and budding areas of the primary and liver metastatic tumors. LGR5$^+$ cells present as a single cell are also found in the interstitium. Similar patterns of the staining were observed in several tumor tissues from different patients. Arrows indicate typical LGR5$^+$ cells, and arrow heads indicate typical LGR5$^-$/EREG$^+$/HLA-DMA$^+$ cells. Bar = 10 μm. **(B):** Ki67 staining of the LGR5$^+$ and the HLA-DMA$^+$ cells in colon cancer tissues from patients. The sections of the primary colon cancer tissues from patients in (A) were double stained with an anti-Ki67 antibody and anti-LGR5 antibody or anti-HLA-DMA antibody. Arrows: LGR5$^+$/Ki67$^+$ cells, Arrow head: HLA-DMA$^+$/Ki67$^-$ cells. Bar = 10 μm. Abbreviation: EREG, epiregulin.

colon cancer tissues, both LGR5$^+$ cells and LGR5$^-$ cells were detected in eight cases, and either LGR5$^!$ or LGR5$^-$ cells were observed in the remaining four cases. The percentages of the LGR5$^+$ and LGR5$^-$ cells in those cases ranged between 0.003% and 1.864% for the LGR5$^!$ and 0.001%–0.243% for the LGR5$^-$ cells (Supporting Information Table S8). Both LGR5$^!$ and LGR5$^-$ cells were detected in ducts and budding areas (Fig. 7A; Supporting Information Table S8). In addition, LGR5$^!$ and LGR5$^-$ cells within the ducts were not restricted to particular regions as they were observed randomly throughout the ducts (Fig. 7A). In budding areas, LGR5$^!$ cells were detected as a single cell or in tumor cell clusters consisting of a few tumor cells (Fig. 7A). Also in clinical specimens, the LGR5$^+$ cells were positive for Ki67, and the LGR5$^-$/HLA-DMA$^+$ cells were negative for Ki67 (Fig. 7B).

Discussion

SC markers such as CD133, CD44, CD166, and ALDH have been used to identify and isolate colon CSCs [25–29]. We observed that colon CSCs reside in subpopulations of the cells positive for these markers; however, none is a definitive marker for colon CSCs. Evidence that Lgr5 marks normal intestinal SCs has accumulated [8, 13]. Despite that evidence, LGR5 remains unexplored in human CSCs, presumably due to a lack of specific antibodies [38]. In this study, we generated monoclonal antibodies that are highly specific to LGR5 and can be applied to immunostaining, flow cytometry, and cell sorting. Using these unique anti-LGR5 antibodies, we were able to define LGR5$^+$ cells as proliferating colon CSCs. To establish pure CSC cell lines, we tested whether spheroid cultures or adherent cultures would be useful to enrich CSCs. Several attempts have been made using spheroid cultures to isolate and enrich CSCs in vitro [9, 14]. The results in this study indicated that spheroid cultures allowed LGR5$^!$ cells to self-renew and differentiate, leading to heterogeneous populations of cells as reported by others [14, 39]. In contrast, adherent cultures kept the LGR5$^!$ cells self-renewing and prevented them from differentiation. Indeed, we did not detect any CK20 expression on the LGR5$^+$ cells during the culture. Thus, the LGR5$^!$ cell lines form a highly homogenous population of cells having CSC properties with strong TIA. Only a few previous reports have described the use of adherent cultures to obtain CSCs such as in glioma and breast cancers [30, 40, 41]. The adherent cultures were rehighlighted to isolate stable cell lines with CSC properties in this study.

Using the established LGR5$^!$ cell lines, definitive evidence for drug-resistant LGR5$^-$ CSC subpopulations was obtained after treatment with anti-cancer drugs such as irinotecan. The LGR5$^+$ cells had a number of CSC characteristics such as self-renewal via symmetric and asymmetric division, TIA, and a pathway for producing a tumor hierarchy of different cell types. In addition, these cell lines transition between two distinct states, an LGR5$^+$ proliferating and an LGR5$^-$ drug-resistant state. Tumor formation from the drug-resistant LGR5$^-$ cells in NOG mice was observed, but the TIA of the drug-resistant LGR5$^-$ cells was slightly lower than that of LGR5$^!$ cells. Drug-resistant LGR5$^-$ cells first converted to LGR5$^!$ cells in the establishment of tumor hierarchy in vivo. The results of irinotecan treatment in vivo suggest that anti-cancer drugs induce transition of LGR5$^!$ cells to drug-resistant cells, and such drug-resistant cells revert to LGR5$^!$ cells after drug treatment is terminated. We could detect both LGR5$^+$ and LGR5$^-$ cells in ducts and budding sites of the tumors reconstituted from either the LGR5$^-$ or LGR5$^+$ cells in mice and also in primary and liver metastasized tumors from patients. These observations may explain why some rare populations of CSCs survive after drug treatments, giving rise to tumor recurrence. If this idea is correct, the CSC cell lines provide a new avenue to test drugs that will kill all of the cancer cells in a tumor.

CSCs self-renew and also give rise to differentiated cancer cells. In fact, the LGR5$^+$ cells exhibited the ability to undergo asymmetric cell divisions, generating two different offspring in vitro and reconstituting tumor hierarchy in vivo. However, it remains unclear whether a transition of differentiated cancer cells to CSCs occurs. Gupta et al. [20] proposed a stochastic state transition of cancer cells. Using breast cancer cell lines, they demonstrated that differentiated cancer cells possessed plasticity and transitioned to CSCs to maintain phenotypic proportions within tumors, although the frequency was very low (between 0.01% and 0.1%). In this study, the colony forming activity of the sorted cells in the 99.4% pure LGR5$^-$/CD133$^-$ population, in which almost all the cells are CSC marker-negative and thereby considered to be differentiated tumor cells, was approximately 0.03%. This number is extremely low but not zero. Therefore, the possibility of a reversion of differentiated cells to CSCs, as proposed by Gupta et al., cannot be ruled out. At the same time, the possibility that colonies were formed by a small number of concomitant LGR5$^!$ cells in this faction also cannot be excluded. Further study which overcomes technological hurdles of cell sorting is necessary to answer this question.

In normal small intestine, the existence of two types of SCs has been described: slow cycling SCs in the +4 position and proliferating SCs in the crypt base [42]. However, the relationship between the two types of SCs was unclear. More recently, Lgr5$^-$/Bmi1$^!$ SCs were shown to serve as a SC pool: they changed to Lgr5$^+$ SCs when the Lgr5$^+$ SCs were absent [15]. Furthermore, Takeda et al. [16] demonstrated the interconversion and bidirectional lineage relationship between proliferating Lgr5$^+$ SCs at the crypt base column and slow cycling SCs that expressed an atypical homeobox protein Hopx at +4 position. Tert, telomerase reverse transcriptase, was reported as molecules that mark predominately noncycling, long-lived intestinal SCs that proliferate upon injury [43]. Powell et al. [44] also demonstrated that expression of Lrig1, a pan ErbB inhibitor, was rather specific to quiescent SCs. However, Wong et al. [45] indicated the coexpression of Lrig1 in Lgr5$^+$ cells, and intensive analysis with DNA microarray and proteomics revealed that Bmi1, Tert, Hopx and Lrig1 were all robustly expressed in Lgr5$^!$ intestinal SCs [46]. In our RT-qPCR analysis, the *HOPX* mRNA was not detected in the LGR5$^+$ and drug-resistant LGR5$^-$ cells, whereas similar levels of the *BMI1* and *LRIG1* mRNA were detected in both LGR5$^!$ and drug-resistant LGR5$^-$ states (Supporting Information Fig. S13). In addition, expression of *TERT* was rather specific to the LGR5$^+$ cells; there was a marked decrease of the *TERT* mRNA after the LGR5$^!$ cells were treated with irinotecan (Supporting Information Fig. S13), which coincided with the results that intestinal SCs contained significant telomerase activity [47]. Except for *HOPX* mRNA expression, we observed expression of the *BMI1*, *LRIG1*, and *TERT* mRNAs in proliferating colon CSCs. Definitive understanding of the physiological roles and the expression of these genes in normal and cancer SCs await further study.

Because localization of proliferating (Lgr5$^!$) and slow cycling quiescent (Lgr5$^-$) SCs is restricted in normal intestine as described above, localization, proliferation, and transition between the slow cycling and proliferating states of SCs may be controlled by niches which include a gradient of the Wnt ligand [42]. The moderately differentiated colon cancers differed from the normal architecture: it showed duct structures

and an epithelial hierarchy, but localization of $LGR5^+$ and $LGR5^-$ cells in ducts appeared not to be restricted to particular regions in both xenotransplanted tumors and in colon cancer tissues in patients, and they were observed throughout ducts. Thus, it seems that in tumor tissues, CSCs undergo proliferation and interconversion of their states without the underlying architecture of gradient producing cells at specific locations in the tissue structure.

It is widely believed that the invasive ability of cancer cells is important for metastasis. In addition, tumor budding is suggested to contribute to metastasis in colon cancer [48]. We could identify three markers—LGR5, HLA-DMA, and EREG—that can mark these CSCs in two distinct states. Because both proliferating and drug-resistant colon CSCs were EREG positive, we addressed whether anti-EREG antibody is efficacious against tumor metastasis. The antibody showed only moderate activity against the established xenograft tumors but exhibited a stronger efficacy in a metastatic model tested in this study, suggesting that the anti-EREG antibody is efficacious in the early stage of cancer development when cancers are rich in CSCs. A number of studies suggest that metastatic nodules arise from rare cells in the primary tumor (CSCs) [49]. If this is correct, then therapies targeting CSCs can have profound effects against metastatic tumors, even greater than upon primary tumors. In this way, the CSC cell lines developed here can give rise to novel therapies that could improve the treatment of cancer patients.

During the review process for this article, three papers appeared providing the evidence for the existence of CSCs in solid tumors in mice: Chen J. et al. (Nature 2012: 488: 522-526), Driessens G. et al. (Nature 2012: 488: 527-530), and Schepers AG et al. (Science 2012: 337: 730-735).

Conclusion

We established human colon cancer cell lines that express LGR5 and possess CSC properties. After treatment of the proliferating $LGR5^+$ cells with an anticancer agent, the $LGR5^+$ cells transition to a drug-resistant $LGR5^-$ state. In addition, the $LGR5^-$ cells converted to an $LGR5^+$ state in the absence of the drug, suggesting a pool of SCs with the ability to interconvert between two distinct states. Using antibodies against LGR5, HLA-DMA, and EREG, we show the existence of $LGR5^+$ and $LGR5^-$ cells in xenotransplanted tumor tissues and in human colon cancer tissues from patients. Furthermore, the anti-EREG antibody exhibited antitumor activity against tumors derived from the $LGR5^+$ cells in a metastatic model. This suggests the physiological importance of CSCs in tumor recurrence. Furthermore, using the anti-EREG antibody, we provide an option for CSC targeting therapy.

Acknowledgments

We thank L.C. Wong, G.N. Yeow, H.S. Ong, Z.X. Wong, and Y. Takai for their technical assistance; Y. Ohnishi, E. Fujii, K. Nakano, Y. Hirata, and K.F-Ouchi for critical discussions; and R. Somerville for proof editing the manuscript. Thanks are also to T. Yamamura and R. Nomura for their continuous support throughout the study. We are also grateful to O. Nagayama, Chairman and CEO of Chugai, for his encouragement. This work is supported in part by a grant from Singapore Economic Development Board.

Disclosure of Potential Conflicts of Interest

S.K., H.Y.O., M.S., O.N., A.K., K.M., M.Y., S.F., K.Y., E.H., Y.W., H.M., M.A., C.K., T.W., T.Yo, and T.Ya. are employees of Chugai Pharmaceutical Co., Ltd. Y.J.C. is employee of PharmaLogicals Research Pte. Ltd. The authors indicate no other potential conflict of interest.

References

1 Shackleton M, Quintana E, Fearon ER et al. Heterogeneity in cancer: Cancer stem cells versus clonal evolution. Cell 2009;138:822–829.
2 Clevers H. The cancer stem cell: Premises, promises and challenges. Nat Med 2011;17:313–319.
3 Vaiopoulos AG, Kostakis ID, Koutsilieris M et al. Concise review: Colorectal cancer stem cells. Stem Cells 2012;30:363–371.
4 Nguyen LV, Vanner R, Dirks P et al. Cancer stem cells: An evolving concept. Nat Rev Cancer 2012;12:133–143.
5 Marusyk A, Almendro V, Polyak K. Intra-tumour heterogeneity: A looking glass for cancer? Nat Rev Cancer 2012;12:323–334.
6 Visvader JE, Lindeman GJ. Cancer stem cells: Current status and evolving complexities. Cell Stem Cell 2012;10:717–728.
7 Magee JA, Piskounova E, Morrison SJ. Cancer stem cells: Impact, heterogeneity, and uncertainty. Cancer Cell 2012;21:283–296.
8 Barker N, Ridgway RA, van Es JH et al. Crypt stem cells as the cells-of-origin of intestinal cancer. Nature 2009;457:608–611.
9 Vermeulen L, Todaro M, de Sousa Mello F et al. Single-cell cloning of colon cancer stem cells reveals a multi-lineage differentiation capacity. Proc Natl Acad Sci USA 2008;105:13427–13432.
10 Takahashi H, Ishii H, Nishida N et al. Significance of Lgr5(+ve) cancer stem cells in the colon and rectum. Ann Surg Oncol 2011;18:1166–1174.
11 Takeda K, Kinoshita I, Shimizu Y et al. Expression of LGR5, an intestinal stem cell marker, during each stage of colorectal tumorigenesis. Anticancer Res 2011;31:263–270.
12 Walker F, Zhang HH, Odorizzi A et al. LGR5 is a negative regulator of tumourigenicity, antagonizes Wnt signalling and regulates cell adhesion in colorectal cancer cell lines. PLoS One 2011;6:e22733.
13 Barker N, van Es JH, Kuipers J et al. Identification of stem cells in small intestine and colon by marker gene Lgr5. Nature 2007;449:1003–1007.
14 Vermeulen L, De Sousa E Melo F, van der Heijden M et al. Wnt activity defines colon cancer stem cells and is regulated by the microenvironment. Nat Cell Biol 2010;12:468–476.
15 Tian H, Biehs B, Warming S et al. A reserve stem cell population in small intestine renders Lgr5-positive cells dispensable. Nature 2011;478:255–259.
16 Takeda N, Jain R, LeBoeuf MR et al. Interconversion between intestinal stem cell populations in distinct niches. Science 2011;334:1420–1424.
17 Quintana E, Shackleton M, Foster HR et al. Phenotypic heterogeneity among tumorigenic melanoma cells from patients that is reversible and not hierarchically organized. Cancer Cell 2010;18:510–523.
18 Sharma SV, Lee DY, Li B, at al. A chromatin-mediated reversible drug-tolerant state in cancer cell subpopulations. Cell 2010;141:69–80.
19 Roesch A, Fukunaga-Kalabis M, Schmidt EC et al. A temporarily distinct subpopulation of slow-cycling melanoma cells is required for continuous tumor growth. Cell 2010;141:583–594.
20 Gupta PB, Fillmore CM, Jiang G et al. Stochastic state transitions give rise to phenotypic equilibrium in populations of cancer cells. Cell 2011;146:633–644.
21 Dieter SM, Ball CR, Hoffmann CM et al. Distinct types of tumor-initiating cells form human colon cancer tumors and metastases. Cell Stem Cell 2011;9:357–365.
22 Lapidot T, Sirard C, Vormoor J et al. A cell initiating human acute myeloid leukaemia after transplantation into SCID mice. Nature 1994;367:645–648.
23 Al-Hajj M, Wicha MS, Benito-Hernandez A et al. Prospective identification of tumorigenic breast cancer cells. Proc Natl Acad Sci USA 2003;100:3983–3988.

24 Singh SK, Hawkins C, Clarke ID et al. Identification of human brain tumour initiating cells. Nature 2004;432:396–401.
25 O'Brien CA, Pollett A, Gallinger S et al. A human colon cancer cell capable of initiating tumour growth in immunodeficient mice. Nature 2007;445:106–110.
26 Ricci-Vitiani L, Lombardi DG, Pilozzi E et al. Identification and expansion of human colon-cancer-initiating cells. Nature 2007;445: 111–115.
27 Dalerba P, Dylla SJ, Park IK et al. Phenotypic characterization of human colorectal cancer stem cells. Proc Natl Acad Sci USA 2007; 104:10158–10163.
28 Huang EH, Hynes MJ, Zhang T et al. Aldehyde dehydrogenase 1 is a marker for normal and malignant human colonic stem cells (SC) and tracks SC overpopulation during colon tumorigenesis. Cancer Res 2009;69:3382–3389.
29 Chu P, Clanton DJ, Snipas TS et al. Characterization of a subpopulation of colon cancer cells with stem cell-like properties. Int J Cancer 2009;124:1312–1321.
30 Mather JP. Concise Review: Cancer stem cells: In vitro models. Stem Cells 2012;30:95–99.
31 Kremer L, Marquez G. Generation of monoclonal antibodies against chemokine receptors. Methods Mol Biol 2004;239:243–260.
32 Todaro M, Alea MP, Di Stefano AB et al. Colon cancer stem cells dictate tumor growth and resist cell death by production of interleukin-4. Cell Stem Cell 2007;1:389–402.
33 Hu Y, Smyth GK. ELDA: Extreme limiting dilution analysis for comparing depleted and enriched populations in stem cell and other assays. J Immunol Methods 2009;347:70–78.
34 Sato Y, Mukai K, Watanabe S et al. The AMeX method. A simplified technique of tissue processing and paraffin embedding with improved preservation of antigens for immunostaining. Am J Pathol 1986;125: 431–435.
35 Suzuki M, Katsuyama K, Adachi K et al. The combination of fixation using PLP fixative and embedding in paraffin by the AMeX method is useful for histochemical studies in assessment of immunotoxicity. J Toxicol Sci 2002;27:165–172.
36 Fujii E, Suzuki M, Matsubara K et al. Establishment and characterization of in vivo human tumor models in the NOD/SCID/gamma(c) (null) mouse. Pathol Int 2008;58:559–567.
37 Buczacki S, Davies RJ, Winton DJ. Stem cells, quiescence and rectal carcinoma: An unexplored relationship and potential therapeutic target. Br J Cancer 2011;105:1253–1259.
38 Barker N, Bartfeld S, Clevers H. Tissue-resident adult stem cell populations of rapidly self-renewing organs. Cell Stem Cell 2010;7:656–670.
39 Emmink BL, Van Houdt WJ, Vries RG et al. Differentiated human colorectal cancer cells protect tumor-initiating cells from irinotecan. Gastroenterology 2011;141:269–278.
40 Pollard SM, Yoshikawa K, Clarke ID et al. Glioma stem cell lines expanded in adherent culture have tumor-specific phenotypes and are suitable for chemical and genetic screens. Cell Stem Cell 2009;4: 568–580.
41 Scheel C, Eaton EN, Li SH et al. Paracrine and autocrine signals induce and maintain mesenchymal and stem cell states in the breast. Cell 2011;145:926–940.
42 Li L, Clevers H. Coexistence of quiescent and active adult stem cells in mammals. Science 2010;327:542–545.
43 Montgomery RK, Carlone DL, Richmond CA et al. Mouse telomerase reverse transcriptase (mTert) expression marks slowly cycling intestinal stem cells. Proc Natl Acad Sci USA 2011;108:179–184.
44 Powell AE, Wang Y, Li Y et al. The pan-ErbB negative regulator Lrig1 is an intestinal stem cell marker that functions as a tumor suppressor. Cell 2012;149:146–158.
45 Wong VW, Stange DE, Page ME et al. Lrig1 controls intestinal stem-cell homeostasis by negative regulation of ErbB signaling. Nat Cell Biol 2012;14:401–408.
46 Muñoz J, Stange DE, Schepers AG et al. The Lgr5 intestinal stem cell signature: Robust expression of proposed quiescent '+4' cell markers. EMBO J 2012;31:3079–3091.
47 Schepers AG, Vries R, van den Born M et al. Lgr5 intestinal stem cells have high telomerase activity and randomly segregate their chromosomes. EMBO J 2011;30:1104–1109.
48 Brabletz T, Jung A, Spaderna S et al. Opinion: Migrating cancer stem cells—An integrated concept of malignant tumour progression. Nat Rev Cancer 2005;5:744–749.
49 Wu X, Northcott PA, Dubuc A et al. Clonal selection drives genetic divergence of metastatic medulloblastoma. Nature 2012;482:529–533.

See www.StemCells.com for supporting information available online.

THE JOURNAL OF BIOLOGICAL CHEMISTRY VOL. 287, NO. 41, pp. 34110–34119, October 5, 2012

Micromanaging Iron Homeostasis

HYPOXIA-INDUCIBLE MICRO-RNA-210 SUPPRESSES IRON HOMEOSTASIS-RELATED PROTEINS[*S]

Received for publication, February 27, 2012, and in revised form, August 14, 2012 Published, JBC Papers in Press, August 15, 2012, DOI 10.1074/jbc.M112.356717

Yusuke Yoshioka[‡§1], **Nobuyoshi Kosaka**[§], **Takahiro Ochiya**[§], **and Takashi Kato**[‡¶2]

From the [‡]*Integrative Bioscience and Biomedical Engineering, Graduate School of Science and Engineering, Waseda University, 2-2 Wakamatsu, Shinjuku, Tokyo 162-8480, Japan, the* [§]*Translational Research Group Division of Molecular and Cellular Medicine, National Cancer Center Research Institute, 5-1-1 Tsukiji, Chuo-ku, Tokyo 104-0045, Japan, and the* [¶]*Department of Biology, School of Education, Waseda University, Tokyo 162-8480, Japan*

Background: The regulatory mechanisms of iron homeostasis in cancer cells are not yet fully understood.
Results: MicroRNA-210 suppresses two essential molecules for iron homeostasis, TfR and ISCU.
Conclusion: Precise regulation of microRNA-210 expression level is vital for maintaining the iron homeostasis, leading to the survival of cancer cells.
Significance: This study reveals the linkages among hypoxia, iron homeostasis, and cancer.

Iron is fundamental for sustaining life for living organisms, and the iron metabolism is finely regulated at different levels. In cancer cells, deregulation of the iron metabolism induces oxidative stress and drives tumor progression and metastasis; however, the molecular mechanisms of iron homeostasis are not fully understood. Here we found that iron deficiency as well as hypoxia promoted microRNA-210 (miR-210) expression. A central mediator of miR-210 transcriptional activation is the hypoxia-inducible factor (HIF)-1α, and the hypoxia-response element in the miR-210 promoter is confirmed experimentally. This is in agreement with the data from *in vivo* studies that have demonstrated the presence of miR-210-expressing cells at the chronic hypoxic regions of xenografted tumors. Furthermore we found two essential molecules for iron homeostasis, iron-sulfur cluster scaffold protein (ISCU) and transferrin receptor 1 (TfR), are a direct target of miR-210. Transfection of miR-210 decreases the uptake of transferrin by inhibiting the expression of TfR. In addition, inhibition of miR-210 by anti-miR-210 up-regulates ISCU expression. These findings suggest that miR-210 works as an iron sensor and is involved in the maintenance of iron homeostasis by sustaining the TfR expression level to stimulate cell proliferation and promote cell survival in the hypoxic region within tumors.

During the evolutionary processes, life has made use of iron in a variety of biochemical processes. For instance, iron is an essential cofactor for nonheme enzymes, such as ribonucleotide reductase, which is essential for DNA synthesis and is also a vital component of the heme in the oxygen-binding protein, hemoglobin (1–3). Iron needs to be tightly regulated, as excess iron is toxic and causes the generation of free radicals (4), whereas iron insufficiency induces hypoferric anemia in mammals (5) coupled to hypoxia in tissues (6, 7). Given the links between iron metabolism and oxygen transport, the associations between the control of the iron concentration and the physiology of the hypoxic response are important (8). Many responses to altered oxygen levels are coordinated by a hypoxia-inducible factor (HIF)[3] (9, 10).

The association between iron and cancer has been shown in animal models and epidemiologic studies in several human cancers. For instance, the oldest reported experiment of iron-induced carcinogenesis is that of mice exposed to iron-oxide dust, which caused pulmonary tumors (11). In addition, various studies have also shown higher levels of expression of the transferrin receptor 1 (TfR), which is an essential protein involved in iron uptake and the regulation of cell growth, in cancer cells than in their normal counterparts (12). TfR could be attributed to the increased need for iron as a cofactor of ribonucleotide reductase involved in the DNA synthesis of rapidly dividing cells. These reports suggest that iron homeostasis is important in cancer initiation and progression. However, the regulatory mechanisms of iron homeostasis in cancer cells are not yet fully understood.

MicroRNAs (miRNAs) have emerged as a new class of non-coding genes involved in regulating a wide variety of biological processes (13, 14), and their mis-expression has been shown to contribute to tumorigenesis (15). Therefore, miRNAs act as

* This work was supported in part by a grant-in-aid for the third-term comprehensive 10-year strategy for cancer control, a grant-in-aid for scientific research on priority areas cancer from the Ministry of Education, Culture, Sports, Science, and Technology, and the Program for Promotion of Fundamental Studies in Health Sciences of the National Institute of Biomedical Innovation (NiBio), the Japan Society for the Promotion of Science (JSPS) through the "Funding Program for World-Leading Innovative R&D on Science and Technology (FIRST Program)," initiated by the Council for Science and Technology Policy (CSTP). This work was supported in part by a grant from the Japan Society for the Promotion of Science (to Y. Y.).
[S] This article contains supplemental Figs. S1–S7.
[1] Supported by a Research Fellowship of the Japan Society for the Promotion of Science for Young Scientists.
[2] To whom correspondence should be addressed: Department of Biology, School of Education and Molecular Physiology Unit Major in Integrative Bioscience and Biomedical Engineering, Graduate School of Science and Engineering, 2-2 Wakamatsu, Shinjuku, Tokyo 162-8480, Japan. Tel.: 81-3-5369-7309; Fax: 81-3-3355-0316; E-mail: tkato@waseda.jp.

[3] The abbreviations used are: HIF, hypoxia-inducible factor; Tf, transferrin; TfR, transferrin receptor 1; miRNA, microRNA; miRNA-210, microRNA-210; ISCU, iron-sulfur cluster scaffold protein; DFO, desferrioxamine; qRT-PCR, quantitative real-time RT-PCR; IRP1, iron regulatory protein 1; NC, negative control.

tuners of gene expression and maintain homeostasis. For instance, miR-144/451 knockout mice display a cell autonomous impairment of late erythroblast maturation, resulting in erythroid hyperplasia, splenomegaly, and mild anemia (16).

In a previous report, we demonstrated that miR-210 is highly expressed in human and murine erythroid cells and in the spleen of mice with hemolytic anemia (17). Erythrocytes require iron to perform their duty as oxygen carriers. Recent reports have shown that the expression of miR-210 is induced by hypoxic conditions (18). Therefore, miR-210 might play an important role in the connection of iron and oxygen. It was already reported that the expression of miR-210 was tightly associated with poor prognosis of breast cancer (18); however, contradictory data exist concerning the regulation and roles of miR-210 during cancer progression. In this study, we clarified that miR-210 regulates iron homeostasis in cancer cells. The expression of miR-210 was induced not only in hypoxic conditions but also in iron deficiency. In addition, we found that the targets of miR-210 are two essential molecules for iron homeostasis, TfR and the iron-sulfur cluster scaffold protein (ISCU). Furthermore, we showed that the distribution of miR-210-expressing cells in inoculated tumor cells could be observed in the chronic hypoxic regions. These results indicated that iron-deficiency-inducible miR-210 controls the expression of two iron regulatory proteins to optimize the survival and proliferation rate of cancer cells located in the chronic hypoxic regions.

EXPERIMENTAL PROCEDURES

Reagents—Rabbit polyclonal anti-ISCU (FL-142) (sc-28860) was purchased from Santa Cruz Biotechnology (Santa Cruz, CA). Mouse monoclonal anti-TfR (13-6800) was purchased from Invitrogen. Mouse monoclonal anti-actin, clone C4 (MAB1501), was purchased from Millipore (Billerica, MA). Mouse monoclonal anti-HIF-1α (610959) was purchased from BD Biosciences. Rabbit monoclonal anti-ferritin (EPR3004Y) was purchased from Epitomics (Burlingame, CA). Rabbit polyclonal anti-ACO1/iron regulatory protein 1 (IRP1) was purchased from Medical & Biological Laboratories Co., Ltd. Rabbit polyclonal anti-red fluorescent protein (ab34771) was purchased from Abcam (Cambridge, MA). Peroxidase-labeled anti-mouse and anti-rabbit antibodies were included in the Amersham Biosciences ECL Plus Western blotting reagents pack (RPN2124) (GE Healthcare). Synthetic hsa-miR-210 (pre-miR-210) and antisense miR-210 oligonucleotide (anti-miR-210) were purchased from Ambion (Austin, TX). The duplexes of each small interfering RNA (siRNA) targeting human HIF-1α mRNA (s30925; target sequences of 5′-GGAGGUGUUUGACAAGCGAdTdT-3′ and 5′-UCGCUUGUCAAACACCUCCtg-3′), an siRNA-specific for human IRP1 (ACO1) mRNA (target sequences of 5′-GCUCGCUACUUAACUAACAtt-3′ and 5′-UGUUAGUUAAGUAGCGAGCag-3′) and negative control 1 (NC1) were purchased from Applied Biosystems. An siRNA-specific for human TfR mRNA (target sequences of 5′-GAACCUGGAUAAUGAUGAAdTdT-3′ and 5′-UUCAUCAUUAUCCAGGUUCdTdT-3′) was purchased from Sigma-Genosys. Desferrioxamine (DFO) was purchased from Calbiochem. Geneticin was purchased from Invitrogen.

Cell Culture—MCF7 cells and MD-MB-231-luc-D3H2LN cells (Xenogen), a human breast cancer cell line, were cultured in RPMI 1640 medium containing 10% heat-inactivated fetal bovine serum (FBS) and an antibiotic-antimycotic (Invitrogen) at 37 °C in 5% CO_2.

Exposure to Hypoxia—Cells were exposed for 24 h or 48 h either to standard nonhypoxic cell culture conditions (20% O_2, 5% CO_2 at 37 °C) or to hypoxia (1% O_2, 5% CO_2 with N_2 balance at 37 °C) in either a modular hypoxia chamber (Wakenyaku) or a tissue culture incubator.

RNA Extraction—RNA was isolated using TRIzol (Invitrogen) and processed according to the manufacturer's instructions.

Quantitative Real-time RT-PCR (qRT-PCR)—Hsa-miR-210 and endogenous control RNU6B TaqMan qRT-PCR kits and human-ISCU, human-TfR, and human-β-actin TaqMan Gene Expression Assays were purchased from Applied Biosystems (Foster City, CA). The reverse transcription and TaqMan quantitative PCR were performed according to the manufacturer's instructions. PCR was carried out in 96-well plates using the 7300 Real-Time PCR System (Applied Biosystems). All reactions were done in triplicate.

The expression levels of pri-miR-210 and β-actin were measured by qRT-PCR using a SYBR Green PCR Master Mix (Invitrogen). Primer sequences are as follows (shown 5′ to 3′): pri-miRNA-210_F, GACTGGCCTTTGGAAGCTCC and R, ACAGCCTTTCTCAGGTGCAG; β-actin_F, GGCACCACCATGTACCCTG and R, CACGGAGTACTTGCGCTCAG.

In Silico MicroRNA Target Prediction—Bioinformatic prediction of target genes and miRNA-binding sites was performed using three programs: TargetScan (version 5.0) (19), Sanger miRBase (version 5) (20), and MirTarget2 (21).

3′-UTR Assay Plasmid Constructs—A 297-bp fragment from the 3′-UTR of ISCU containing the predicted target sequence of miR-210 (located at positions 102–109 of the ISCU1/2 3′-UTR) and a 385-bp fragment from the 3′-UTR of TfR containing the predicted target sequence of miR-210 (located at positions 229–235 of this fragment) were PCR-cloned from MCF7-isolated total RNA. Three prime A-overhang was added to the PCR products after 15 min of regular *Taq* polymerase treatment at 72 °C. The PCR products were cloned into a pGEM-T Easy Vector (Promega; Madison, WI). A pair of primers including XhoI and NotI restriction sites was designed to amplify the 3′-UTR of ISCU and TfR insert. The amplified products were ligated into the XhoI and NotI sites of the 3′-UTR of the *Renilla* luciferase gene in the psi-check-2 plasmid (Promega) to generate psi-ISCU and psi-TfR. Primer sequences are as follows (shown 5′ to 3′): ISCU_F, GCTCGAGTAACTCCGTTACTTCCAGCAGGC and ISCU_R, GCGGCCGCTAATATGCACTTCACGGGCTATC; TfR_F, GCTCGAGTAATCAGCTGTTTGTCATAGGGC and TfR_R, GCGGCCGCTAGGTCATGCACGATTGTCCGA. Site-directed mutagenesis or deletion mutant was performed in the seed sequences of ISCU and TfR. PrimeStar Max DNA Polymerase (Takara; Kyoto, Japan) was used for PCR amplification. Forward primer and reverse primer sequences are as follows (shown 5′ to 3′): ISCU_mut_F, AGATGTATGTGGTACTTGCTGTTCACGTTA and ISCU_mut_R, GTACCACATACAT-

CTCATAGCTCTTCGGT; ISCU_del_F, ATGAGATTACTTGCTGTTCACGTTA and ISCU_del_R, GCAAGTAATCTCATAGCTCTTCGGT; TfR_mut_F, TGTTGCACGCGCGTACTTAAATGAAAGCA and TfR_mut_R, TACGCGCGTGCAACACCCGAACCAGGAAT; TfR_del_F, CGGGTGTTCGTACTTAAATGAAAGCA and TfR_del_R, AAGTACGAACACCCGAACCAGGAAT.

Immunoblot Analysis—SDS-PAGE gels were calibrated with Precision Plus Protein standards (161-0375) (Bio-Rad), and anti-HIF-1α (1:500), anti-ISCU (1:200), anti-TfR (1:500), and anti-actin (1:1000) were used as primary antibodies. The dilution ratio of each antibody is indicated in parentheses. Two secondary antibodies (peroxidase-labeled anti-mouse and anti-rabbit antibodies) were each used at a dilution of 1:10,000. Bound antibodies were visualized by chemiluminescence using the ECL Plus Western blotting detection system (RPN2132) (GE Healthcare), and luminescent images were analyzed with a LuminoImager (LAS-3000; Fuji Film Inc.).

Flow Cytometric Analysis—MCF7 cells and MDA-MB-231-luc-D3H2LN cells were transfected with pre-miR-210 or pre-NC. After culturing for 48 h, transfected cells were serum-starved for 30 min and then incubated for 45 min in a serum-free medium containing 50 μg of transferrin/ml conjugated with Alexa Fluor 594 (Invitrogen). Transfected cells were suspended in their culture medium and subjected to a FACSAria II cell sorter (BD Biosciences). At least one million cells were pelleted by centrifugation at 180 × *g* for 5 min at 4 °C, resuspended in a 20 μl of a monoclonal mouse anti-human CD71-FITC antibody (BD Biosciences, clone M-A712), and incubated for 30 min at 4 °C. Three independent experiments were performed.

Transferrin-uptake Analysis—Transferrin-uptake experiments were performed 48 h after transfection with pre-miR-210 or pre-NC. Transfected cells were serum-starved for 30 min and then incubated for 45 min in a serum-free medium containing 50 μg of transferrin/ml conjugated with Alexa Fluor 594. Cells were then washed and fixed in 4% paraformaldehyde for 15 min at room temperature. After washing with PBS, they were incubated with mouse anti-TfR antibody diluted 1:100 in Dako REAL Antibody Diluent (Dako; Carpinteria, CA) for 1 h. They were then incubated with Alexa Fluor 488 goat anti-mouse IgG diluted 1:1000 in Dako REAL Antibody Diluent for 45 min. Finally, the cells were stained with the fluorescent DNA-binding dye Hoechst 33342 (Invitrogen) for 5 min.

Establishment of Stable Cell Lines—Stable knockdown of ISCU MCF7 cell lines was generated by selection with 4 μg/ml blasticidine (Invitrogen). MCF7 cells were transfected with 0.5 mg of an siISCU1/2 vector or a negative control vector at 90% confluence in 24-well dishes using a Lipofectamine LTX reagent in accordance with the manufacturer's instructions. After 24 h, the cells were replated in a 10-cm dish followed by 3-week selection with 4 μg/ml blasticidine.

Immunohistochemical Staining—Between all consecutive steps of the staining procedure, the sections were rinsed three times for 5 min in PBS. The sections were first fixed in 10% formalin for 4 h. After re-hydration of the tissue sections in PBS for 1 h, they were incubated with mouse anti-HIF-1α diluted 1:500 and rabbit anti-red fluorescent protein diluted 1:100 in Dako REAL Antibody Diluent for 1 h. Sections were then incubated with Alexa Fluor 488 goat anti-mouse IgG and Alexa Fluor 594 goat anti-rabbit IgG (Molecular Probes; Leiden, The Netherlands) diluted 1:1000 in Dako REAL Antibody Diluent for 45 min. Finally, sections were mounted on ProLong Gold antifade reagent with DAPI (Invitrogen).

In Vivo miR-210-monitoring Assay—The pDsRed-Express-DR vector (Clontech Laboratories), which is a promoterless vector that encodes DsRed-Express-DR, was purchased from Takara Bio. This protein is a destabilized variant of the red fluorescent protein. For miR-210 promoter-driven fluorescent-based reporter assays, pmiR-210-DsRed was constructed by inserting a miR-210 promoter region into a multi-cloning site of pDsRed-Express-DR vector at HindIII and XhoI sites. A sensor vector for miR-210 was constructed by introducing tandem binding sites with a perfect complementarity sequence to miR-210, separated by a four-nucleotide spacer into the NotI site of pDsRed-Express-DR vector, which already introduced the CMV promoter into the multi-cloning site. The sequences of the binding site are as follows: 5′-AGTGATTCAGCCGCTGTCAC***ACGCACA***GACGCGTTCAGCCGCTGTCAC***ACGCACA***GATCGAA-3′ (sense) and 5′-TTCGATC***TGTGCGT***GTGACAGCGGCTGAACGCGTC***TGTGCGT***GTGACAGCGGCTGAATCACT-3′ (antisense). The seed sequence of miR-210 is indicated in bold italics. All plasmids were verified by DNA sequencing.

Statistical Analysis—Data presented as *bar graphs* are the means ±S.E. of at least three independent experiments. Statistical analysis was performed using Student's *t* test.

RESULTS

Iron Deficiency Induces the Expression of miR-210 through the HIF-1α, and miR-210 Directly Suppresses ISCU—To try to determine the possible contribution of miR-210 in the regulation of iron homeostasis, we first measured the expression of miR-210 in breast cancer cells, MCF7 and MDA-MB-231 (MM231) cells, and human breast epithelial cells, MCF10A, after treatment with an iron chelator, DFO. The expression level of miR-210 was increased 3–5-fold above basal levels by the 48 h of DFO treatment compared with untreated cells (Fig. 1*A*). In addition, excess amounts of iron by addition of 500 mM ferric ammonium citrate had no effect on the induction or suppression of the expression of miR-210. To further analyze whether the biogenesis of miR-210 during iron depletion is regulated by a transcriptional mechanism or processing machinery of miRNA biogenesis, we quantified the expression of primary miR-210 (pri-miR-210) in MCF7 cells. The expression of pri-miR-210 levels was induced 1.5–3.5-fold above basal levels by the DFO treatment compared with untreated cells (Fig. 1*B*). This result indicated that the induction of miR-210 is because of transcriptional regulation. As shown previously, the transcription of miR-210 was regulated by iron-deficient-induced HIF-1α through the binding of hypoxia-responsible elements that are located upstream of the miR-210 gene (22) (supplemental Fig. S1, *A–D*). Indeed, suppression of HIF-1α by siRNA (supplemental Fig. S1*E*) leads to a significant reduction of miR-210 expression after treatment with DFO (Fig. 1*C*).

Recent reports showed that miRNAs play a role in feedback and feed-forward transcriptional regulation (23, 24). Previ-

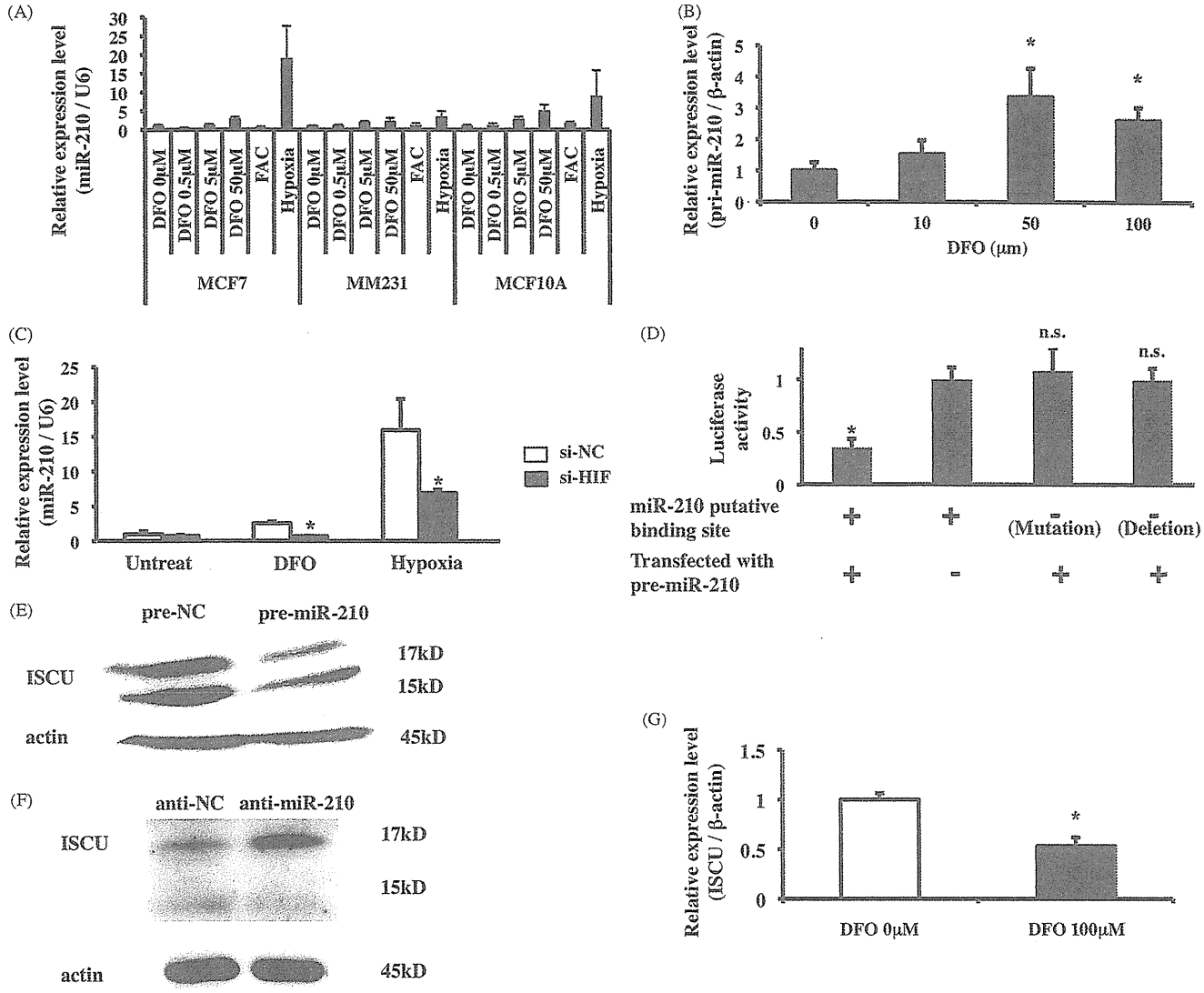

FIGURE 1. **Expression of miR-210 is induced by iron deficiency, and target gene of miR-210 is ISCU.** *A*, miR-210 expression was detected by qRT-PCR after treatment with various concentrations of DFO or exposure to 1% O_2 for 48 h. RNU6B was used as a control. *B*, primary miR-210 expression was detected by qRT-PCR after treatment with DFO for 48 h. β-Actin was used as a control. *C*, MCF7 cells were transfected with HIF-1α siRNA or control siRNA and treatment with DFO 50 μM or exposure to 1% O_2 for 24 h. miR-210 expression was detected by qRT-PCR. RNU6B was used as a control. *, $p < 0.05$ compared with control siRNA groups. *D*, MCF7 cells were co-transfected with pre-miR-210 or pre-NC and psi-ISCU or with its mutant or deletion vector. After 48 h, luciferase activities were measured. *, $p < 0.05$ compared with pre-NC. *n.s.*, not significant. *E*, MCF7 cells were transfected with pre-miR-210 or pre-NC. After 48 h, ISCU expression was detected by immunoblotting. Actin was used as a loading control. *F*, MCF7 cells were transfected with anti-miR-210 or anti-NC and exposed to 1% O_2. After 48 h, ISCU expression was detected by immunoblotting. Actin was used as a loading control. *G*, ISCU expression was detected by qRT-PCR after treatment with DFO 100 μM for 48 h. *, $p < 0.05$ compared with untreated cells. β-Actin was used as a control.

ously, we reported that miR-210 is involved in the production of erythrocytes, which consume 70% of body iron in humans and are the major carriers of oxygen (17, 25). Based on those reports and our finding that the expression of miR-210 was regulated by the iron concentration through the activation of HIF-1α in this study (Fig. 1, *A–C*, and supplemental Fig. S1), we hypothesized that miR-210 regulates genes that are associated with a potent iron homeostasis and a hypoxic cellular response. According to these criteria, ISCU was predicted as a miR-210 target by miRNA target prediction algorithm programs (supplemental Fig. S2*A*). ISCU is an essential factor of the mitochondria electron transport chain, and loss of function of ISCU can disrupt iron homeostasis (26). Although ISCU was known to be regulated by miR-210 in hypoxic condition (27, 28), the precise mechanism of miR-210 on iron homeostasis in cancer cells has not been clarified yet. As shown in Fig. 1*D*, miR-210 recognized the 3′-UTR of ISCU. On the contrary, miR-210 seed sequence in the 3′-UTR of ISCU was mutated or deleted, miR-210 could not bind to the 3′-UTR of ISCU (Fig. 1*D*). In addition, overexpression or knockdown of miR-210 in MCF7 cells down-regulated or up-regulated the expression of ISCU assessed by qRT-PCR (supplemental Fig. S2, *C* and *D*) and immunoblotting (Fig. 1, *E* and *F*). These results are consistent with previous findings that ISCU was a direct target of miR-210. To understand the contribution of miR-210 and ISCU on iron homeostasis in breast cancer cells, we checked the expression of ISCU under the condition of iron depletion in breast cancer cells. As shown in Fig. 1*G*, the expression of ISCU was down-regulated after the treatment with DFO, suggesting that the expression of ISCU was controlled by iron-deficient-induced miR-210 in breast

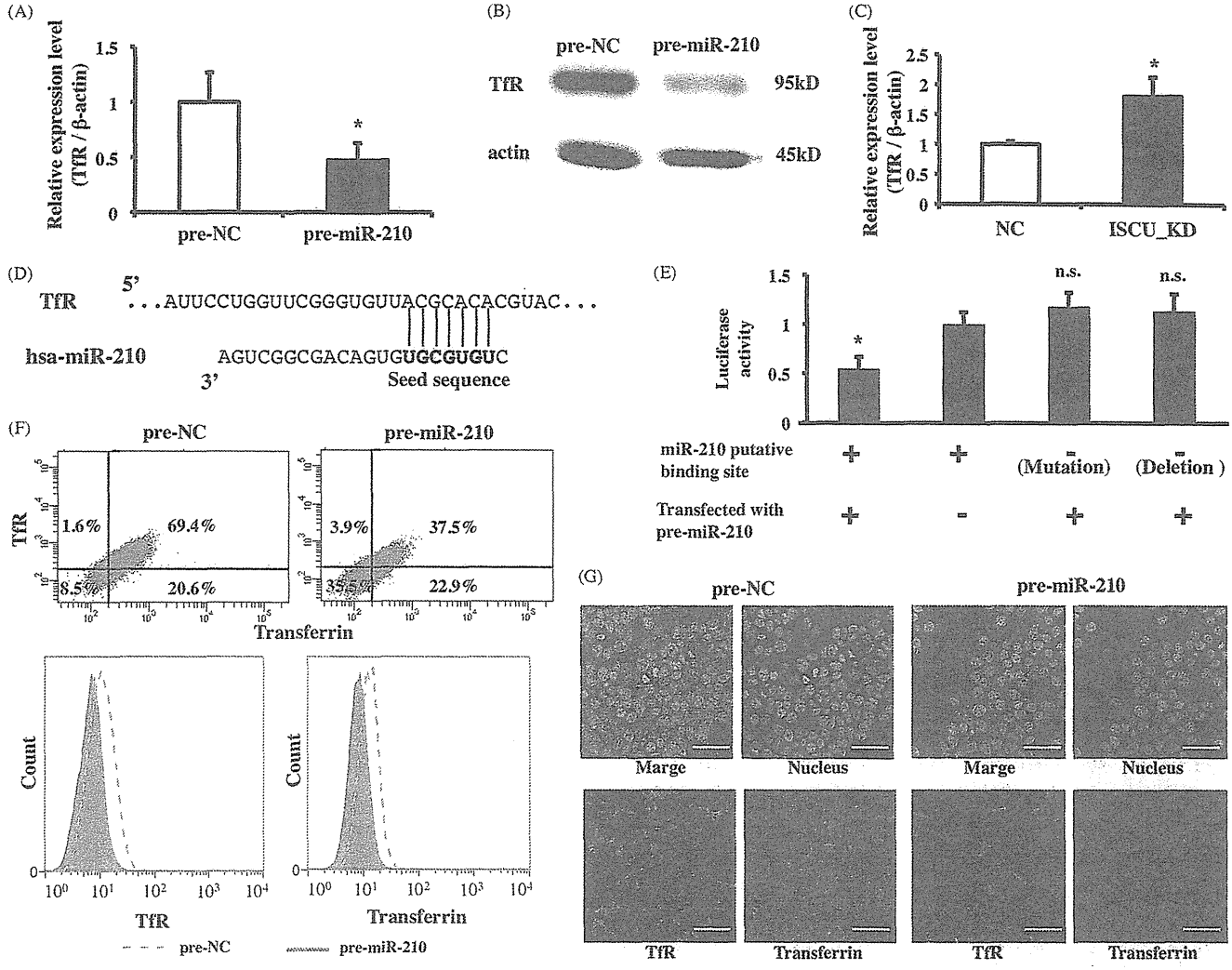

FIGURE 2. **miR-210 also represses the expression of TfR as a target gene.** *A*, MCF7 cells were transfected with pre-miR-210 or pre-NC. After 48 h, TfR expression was detected by qRT-PCR. β-Actin was used as a control. *, $p < 0.05$ compared with pre-NC. *B*, MCF7 cells were transfected with pre-miR-210 or pre-NC. After 48 h, TfR expression was detected by immunoblotting. Actin was used as a loading control. *C*, expression of TfR is increased by knockdown of ISCU. TfR expression was detected in ISCU knockdown cells by qRT-PCR. β-Actin was used as a control. *ISCU_KD*, ISCU knockdown cell line; *NC*, control cell line. *, $p < 0.05$ compared with the control group. *D*, the predicted binding site for miR-210 at 3′-UTR of TfR gene is shown. The *bold font* shows the seed sequence of miR-210. *E*, MCF7 cells were co-transfected with pre-miR-210 or pre-NC and psi-TfR or with its mutant or deletion vector. After 48 h, luciferase activities were measured. *, $p < 0.05$ compared with pre-NC. *n.s.*, not significant. *F*, MCF7 cells were transfected with pre-miR-210 or pre-NC. After 48 h, transfected cells were incubated with Alexa Fluor 594-labeled Tf for 45 min. Expression of TfR (*y* axis) and uptake of transferrin (*x* axis) (*upper panel*) were analyzed by FACS. The *right lower panel* represents the expression of TfR. The *left lower panel* represents uptake of transferrin. *Dashed histogram*, transfected pre-NC; *filled histogram*, transfected pre-miR-210. *G*, MCF7 cells were transfected with pre-miR-210 or pre-NC. After 48 h, transfected cells were incubated with Alexa Fluor 594-labeled Tf (*red*) for 45 min and fixed in 4% paraformaldehyde for 30 min. Subsequently, cells were immunostained using anti-TfR antibody and an Alexa Fluor 488-conjugated secondary antibody (*green*). The nucleus was then stained with the Hoechst 33342 (*blue*). *Scale bar*, 50 μm.

cancer cells. These results prompted us with the idea that iron-ISCU pathway might regulate the iron homeostasis in breast cancer cells.

miR-210 Suppresses the Major Iron-uptake Protein TfR—In mammalian cells, knockdown of ISCU markedly reduces mitochondrial aconitase activity and then promotes the activity of IRP1. Activation of IRP1 accelerates the binding to multiple iron-responsive elements in the 3′-UTR of the mRNA, such as TfR involved in iron acquisition, then leading to increased mRNA stability (26). When IRP1 binds to the 3′-UTR of TfR mRNA, which is an iron-uptake protein, the transcript is protected from degradation. Therefore, we hypothesized that overexpression of miR-210 stabilizes mRNA of TfR via the activation of IRP1. To prove this hypothesis, we measured the expression of mRNA and the protein level of TfR after transfection of the miR-210 mimic (pre-miR-210) in MCF7 and MM231 cells. Surprisingly, the expression of TfR was down-regulated after the transfection of pre-miR-210 (Fig. 2, *A* and *B*, and supplemental Fig. S4*A*). This is an unexpected result because the expression of TfR was increased in ISCU stably knockdown cells (Fig. 2*C* and supplemental Fig. S2*E*). Those results led us to consider that miR-210 directly suppressed the expression of TfR by binding to the 3′-UTR of TfR. To check whether or not TfR is a direct target gene of miR-210, we once again used *in silico* algorithms and found that there was an miR-210-binding site at 3′-UTR of TfR (Fig. 2*D*). To prove that miR-210 directly recognizes the identical predicted target site in the 3′-UTR of TfR, MCF7 cells were transfected with psi-TfR, which was fused to 3′-UTR of TfR and the luciferase open reading frame, or a control vector. In addition, we also prepared

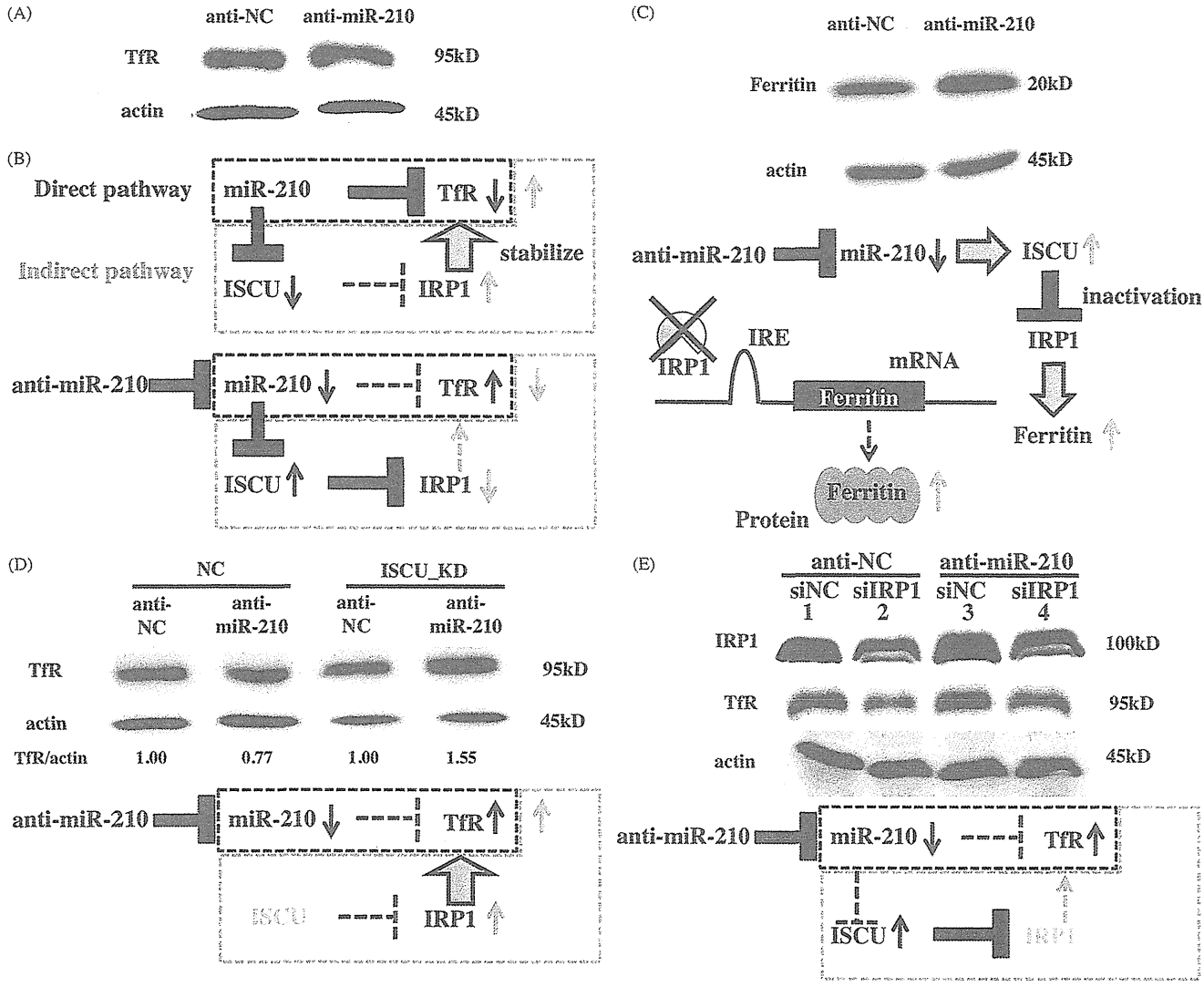

FIGURE 3. **miR-210 has two pathways for regulating TfR expression.** *A*, MCF7 cells were transfected with anti-miR-210 or anti-NC and exposed to 1% O_2 for 48 h. TfR expression was detected by immunoblotting. Actin was used as a loading control. *B*, schematic represents the regulation of two miR-210 target genes after treatment with anti-miR-210. After the transfection of anti-miR-210, the expression of TfR was indirectly decreased via the up-regulation of ISCU. On the other hand, the expression of TfR was directly increased through the down-regulation of miR-210. The expression of TfR then seemed to be unchanged after the transfection of anti-miR-210. *Direct pathway* means that miR-210 recognized the 3′-UTR of TfR and directly (see *black box*) regulates its expression. On the other hand, *Indirect pathway* means that miR-210 indirectly regulates TfR expression through the ISCU-IRP1 pathway (see *gray box*). After the transfection of anti-miR-210 (see *lower panel*), the expression of miR-210 was down-regulated, and then the expression of TfR was up-regulated (see *black box*). On the other hand, expression of ISCU was up-regulated after the transfection of anti-miR-210, and then the activity of IRP1 was inhibited by up-regulation of ISCU: IRP1 was important for the translation of TfR. Thus, inhibition of IRP1 activity by up-regulation of ISCU results in the down-regulation of TfR (see *gray box*). *C*, MCF7 cells were transfected with anti-miR-210 or anti-NC and exposed to 1% O_2. After 48 h, ferritin expression was detected by immunoblotting. Actin was used as a loading control. *Lower panel* shows schematic representation of the regulation of miR-210 target gene and ferritin after treatment with anti-miR-210. *D*, ISCU knockdown cell lines were transfected with anti-miR-210 or anti-NC and exposed to 1% O_2 for 48 h. TfR expression was detected by immunoblotting and quantified by densitometry. Actin was used as a loading control. *Lower panel* shows schematic representation of the regulation of miR-210 target gene after treatment with anti-miR-210 in *ISCU_KD* cells. Because ISCU was stably suppressed by shRNA in these cells, the activity of IRP1 was increased (*gray box*). Therefore, in this experiment, TfR was up-regulated by not only the down-regulation of miR-210 that directly targets the TfR but also the activation by IRP1. *E*, MCF7 cells were transfected with anti-miR-210 or anti-NC and siIRP1 or siNC and exposed to 1% O_2 for 48 h. Expression of IRP1 (*upper*) and TfR (*middle*) was detected by immunoblotting. Actin was used as a loading control. *Lower panel* shows schematic representation of the regulation of miR-210 target gene after treatment with anti-miR-210 and siIRP1. Because the expression of IRP1 was suppressed by siRNA, there is no influence on the TfR expression by *Indirect pathway* (*gray box*). On the other hand, the expression of miR-210 was down-regulated by anti-miR-210. As a result, TfR was up-regulated in this experiment.

psi-TfR_mut, which has a mutated sequence of a putative miR-210-binding site or psi-TfR_del, which has deleted a putative miR-210-binding site. Co-transfection of pre-miR-210 down-regulated *Renilla* luciferase activity significantly more than in pre-NC in the presence of psi-TfR. In contrast, *Renilla* luciferase activity was not altered in the presence of psi-TfR_del or psi-TfR_mut (Fig. 2*E*). We confirmed that miR-210 targets the 3′-UTR of TfR mRNA, showing that miR-210 directly suppresses not only ISCU but also TfR. TfR plays a major role in cellular iron uptake through binding to and internalizing a carrier protein transferrin (Tf). Therefore, to examine whether reduction of TfR by transfected pre-miR-210 functionally inhibited the uptake of Tf or not, Alexa Fluor 594-labeled Tf was used to monitor the uptake of Tf by immunostaining and FACS analysis. As shown in Fig. 2, *F* and *G*, uptake of Tf was lower in pre-miR-210-transfected cells than in control cells,

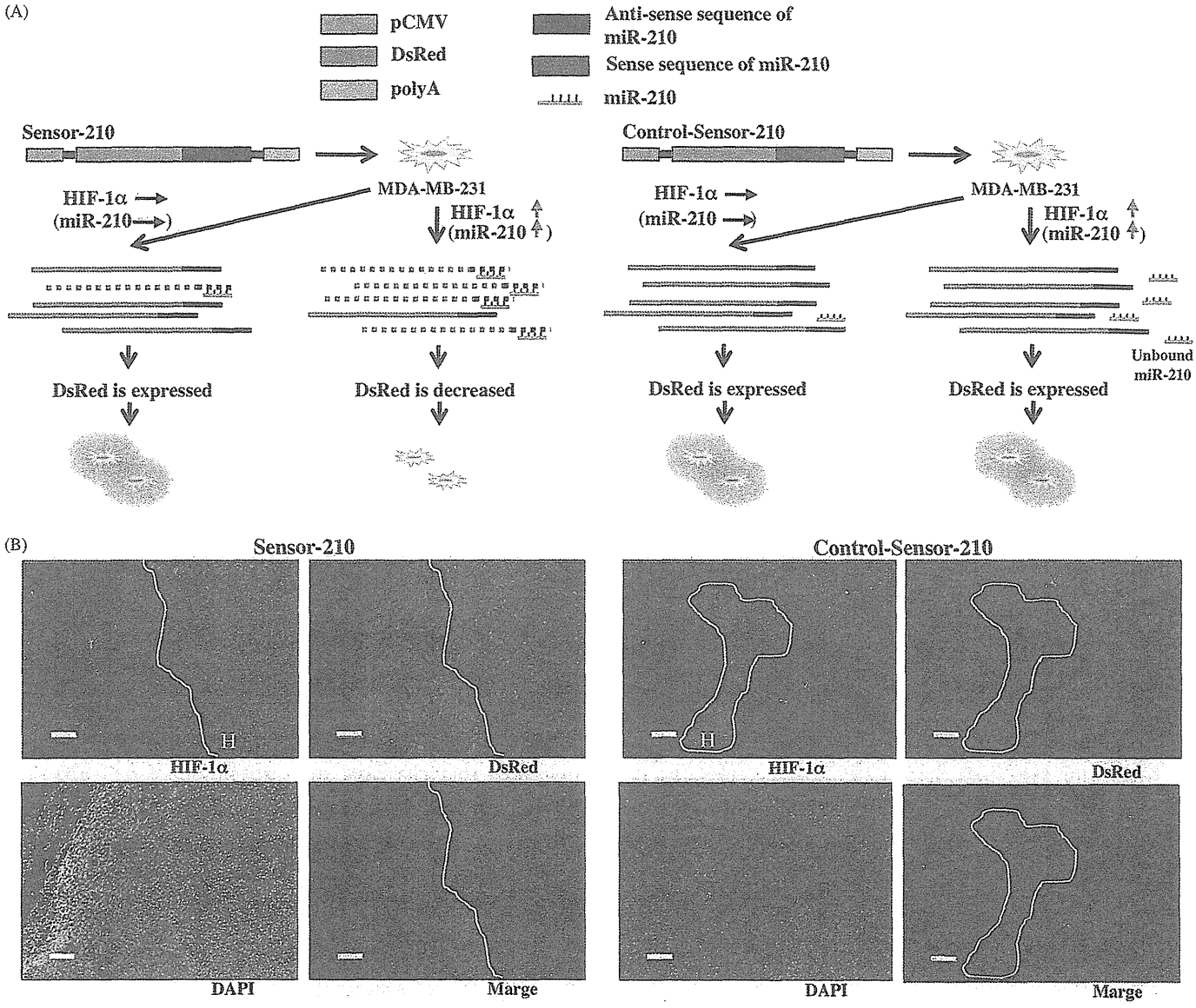

FIGURE 4. **miR-210-expressing cells were localized in the chronic hypoxic region of inoculated tumor cells.** *A*, schematic represents miR-210 tracing assay. In the hypoxic condition, expression of miR-210 is increased by the HIF-1, and then the transcripts of DsRed are degraded by miR-210 (*dashed lines with red and black*). On the other hand, expression of miR-210 is not changed under the normoxic condition (*lines with red and black*). In addition, the fluorescence of Control-Sensor-210 was not changed even under hypoxic conditions. Because their miR-210-binding sites were inserted inversely, the miR-210 could not bind to the 3′-UTR of DsRed. *B*, immunohistochemical analysis of DsRed in the tumor is shown. Sections were stained with the rabbit polyclonal anti-red fluorescent protein antibody and the mouse monoclonal anti-HIF-1α antibody. The fluorescence of DsRed could not be observed in HIF-1α-positive regions in the Sensor-210-inoculated tumor; on the other hand, there was uniform fluorescence of DsRed in Control-Sensor-210-cells-inoculated tumor. *H*, hypoxic region in a tumor is indicated. *Scale bar*, 100 μm.

indicating a direct correlation between TfR reduction and the decreased uptake of Tf in miR-210-overexpressing cells (Fig. 2, *F* and *G*). We also confirmed similar results using an MM231 cells (supplemental Fig. S4, *B* and *C*). Consequently, these observations indicated that overexpression of miR-210 decreases the concentration of intracellular iron by inhibiting the Tf-TfR-dependent iron-uptake system.

miR-210 Is a Member of Iron Homeostatic Networks—As shown in Fig. 2, overexpression of miR-210 inhibited the uptake of Tf via the suppression of TfR. However, because overexpression of miR-210 by miR-210 mimics transduces an extremely high amount of miRNA in the cells (supplemental Fig. S3*A*), it is necessary to examine the function of miR-210 in iron homeostasis under physiological conditions. To evaluate the physiological relationship among miR-210, ISCU, and TfR expression, we transfected antisense miR-210 oligonucleotide (anti-miR-210), which suppresses the expression of miR-210 (supplemental Fig. S3*B*) and control oligonucleotide (anti-NC) into MCF7 cells under a hypoxic condition. We observed the induction of ISCU expression level after the transfection of anti-miR-210 (Fig. 1*F* and supplemental Fig. S2*D*); however, the expression of TfR was not affected (Fig. 3*A* and supplemental Fig. S5*A*). The knockdown of ISCU has been known to increase the expression of TfR by activating IRP1 activity (Fig. 2*C*) (26). From these observations, we assumed that unchanged TfR expression after the transfection of anti-miR-210 was caused by the up-regulation of the ISCU expression level by anti-miR-210 (Fig. 3*B*), leading to the inhibition of IRP1 activity without affecting the

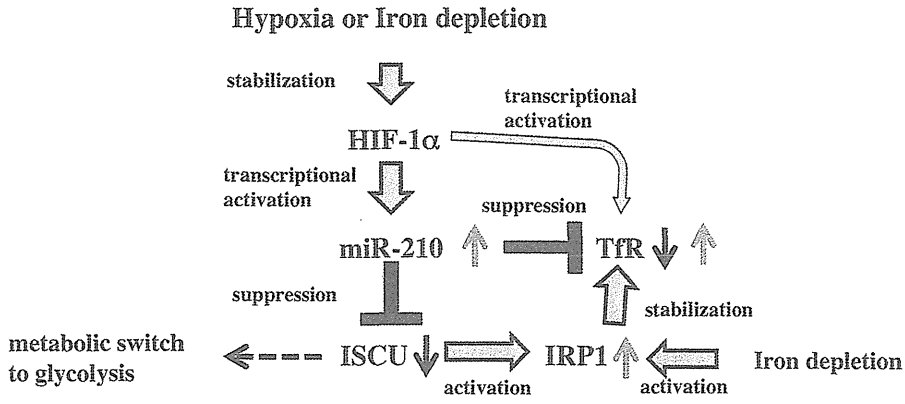

FIGURE 5. **Schematic representation of our proposed model.** miR-210 is induced by hypoxia and iron depletion and directly suppresses two iron homeostasis-related proteins. miR-210 regulates the iron homeostasis with dual pathways of regulating TfR expression. The *gray arrows* indicate up-regulation, and the *black arrows* indicate down-regulation. The *dashed arrow* indicates shift to metabolic switch.

IRP1 expression level. To confirm the change of IRP1 activity by miR-210 expression level in our experiment, we transfected anti-miR-210 or pre-miR-210 into MCF7 cells and analyzed the expression level of ferritin protein, which is the iron storage protein, by immunoblotting. Because the 5′-UTR of ferritin mRNA contains a single iron-responsive element that affects translation initiation, inhibition of IRP1 activity led to the up-regulation of ferritin expression (29). Indeed, the expression level of ferritin was increased in anti-miR-210-transfected cells compared with that in anti-NC-transfected cells (Fig. 3*C*). On the other hand, overexpression of miR-210 by pre-miR-210 suppressed the expression of ferritin in MCF7 cells, indicating that the activity of IRP1 was modulated by miR-210 through ISCU pathway (supplemental Fig. S5*B*). To eliminate the effect of ISCU on TfR expression in this assay system, we established stable ISCU knockdown cell lines using the MCF7 cell. In ISCU knockdown cells, the expression of TfR was higher than that in control cells by activated IRP1 (Fig. 2*C* and supplemental Fig. S2*E*). We carried out the same experiment as shown in Fig. 3*A* using ISCU knockdown cell lines and observed that anti-miR-210 increased TfR mRNA and protein level in ISCU knockdown cell lines but not in control cell lines (Fig. 3*D*). This result indicated that the expression of TfR was up-regulated by not only the down-regulation of miR-210 that directly target the TfR but also the activated IRP1, which is usually inactivated by ISCU. Furthermore, MCF7 cells were transfected with siRNA against IRP1 (or siNC) and anti-miR-210 (or anti-NC) under hypoxic condition, and these cells were analyzed for the expression of IRP1 and TfR by immunoblotting. As a result, because the IRP1 is known to stabilize the TfR mRNA, knockdown of IRP1 by siRNA caused a decrease in the expression of TfR (Fig. 3*E*; compare *lanes 1* and *2*). Importantly, co-transfection of anti-miR-210 and IRP1 siRNA induced the expression of TfR, indicating that miR-210 directly targets the TfR in cancer cells (Fig. 3*E*; compare *lanes 2* and *4*). Taken together, these data suggest that miR-210 regulates TfR expression through direct and indirect translational regulatory mechanisms to fine-tune the iron homeostasis (Fig. 3*B*).

The Distribution of miR-210-expressing Cells Is Associated with Chronic Hypoxia—Most tumors have lower median O_2 partial pressures than their tissue of origin and are deprived of nutrients, including iron (30). Significant variations in these relevant parameters must be expected between different locations within the same tumor at the same location at different times and between individual tumors of the same grading and staging. Previous results have shown that the expression of miR-210 is modulated by the cellular iron concentration and oxygen tension; however, what kinds of cells *in vivo* expressed miR-210 have not been clarified yet. For this reason, we postulated that clarifying the distribution of miR-210-expressing cells in the tumor leads to the understanding of cancer metabolism regulated by iron concentration. To answer this, we investigated the distribution of miR-210-expressing cells in an *in vivo* breast tumor xenograft model. In this experiment, we prepared the cell line, called MDA-MB-231-miR-210-sensor, to trace the expression of miRNA-210 *in vivo*. Because this cell was established by DsRed harboring a complementary sequence of miR-210, the fluorescence of DsRed was diminished when the expression of miR-210 was induced (Fig. 4*A* and supplemental Fig. S6*A*). We injected 5×10^6 MDA-MB-231-miR-210-sensor cells into nude mice. Prior to the excision of tumors, the mice were administered pimonidazole, a compound that binds irreversibly to hypoxic cells (31). Serial sections of the tumors were subsequently stained for pimonidazole, HIF-1α, and DsRed. A correlation between HIF-1α-positive cells and DsRed-negative cells, indicative of diminishment of DsRed expression by miR-210, was observed at the hypoxic rim around necrotic regions of the tumor, a location typically associated with chronic hypoxia (Fig. 4*B*). We also observed that pimonidazole-positive cells and DsRed-negative cells overlapped. On the other hand, fluorescence of control-miR-210-sensor cells, whose miR-210-binding site was inserted inversely with the miR-210-sensor vector, was not changed in inoculated tumor cells. Furthermore, we also established a cell line that enabled us to trace the expression of miR-210 by its promoter-driven DsRed (Fig. S6*B*) and obtained similar results with the MDA-MB-231-miR-210-sensor (Fig. S6*C*). Together, these observations indicated that the expression of miR-210 was

increased in the severely hypoxic region of the tumor. Namely, miR-210 regulates the iron homeostasis in cancer cells under the chronic hypoxic condition in tumors.

DISCUSSION

Iron is indispensable for the function of many prosthetic groups, whereas excess free iron can oxidize and damage the protein, nucleic acid, and lipid contents of cells. Thus, animals evolved complex mechanisms to control the favorable concentrations of intracellular iron. In this study, we revealed that miR-210 is involved in a novel iron homeostasis mechanism through the association of ISCU and TfR in cancer cells (Fig. 5). miR-210 down-regulates ISCU and the Fe-S cluster to mediate the energy metabolic shift from aerobic oxidative phosphorylation to anaerobic glycolysis (32). Concurrently, reduction of the Fe-S cluster activates IRP1, and, subsequently, the expression of TfR is increased, resulting in the elevated uptake of the iron ion. However, several reports show that the excess iron can be toxic (4). To reduce the cellular iron concentration, miR-210 directly suppresses the expression of TfR. Thus, miR-210 regulates iron homeostasis and avoids intracellular iron toxicity.

Compared with normal cells, cancer cells require a large amount of iron; thus, they generally proliferate at a larger rate than their normal counterparts. Hence, iron chelators exert their anti-proliferative effects on tumors (12). Moreover, a previous report showed that down-regulation of TfR decreased cellular proliferation and altered expression of genes involved in cell cycle control (33). Thus, as summarized in Fig. 5, it is postulated that miR-210 has two pathways for the regulation of TfR expression. One is the TfR up-regulation pathway via suppression of ISCU (indirect pathway), and the other one is the TfR down-regulation pathway by direct binding to TfR mRNA. Reduction of ISCU only increases the binding activity of IRP1, but its level of expression does not change. Thus, the effect of up-regulation of TfR by reduced ISCU depends on the amount of IRP1 protein. There are limitations to the up-regulation of TfR by the indirect pathway. Then, in the case of a further increase of miR-210, direct suppression of TfR is superior to its up-regulation by the indirect pathway. In other words, because the forced expression of miR-210 overwhelms the indirect pathway, the direct pathway is superior to the indirect one. Therefore, exogenous transfection of miR-210 causes TfR suppression (Fig. 2), thereby reducing cellular proliferation (supplemental Fig. S7) (34, 35). Moreover, we confirmed the overlap of chronic hypoxic regions and miR-210-expressing cells in inoculated cancer cells *in vivo*. These observations suggest that precise regulation of miR-210 expression level is vital for maintaining the iron homeostasis, leading to the survival and proper cellular proliferation of cancer cells.

HIFs and IRPs are key mediators of cellular iron homeostasis and oxygen, respectively. Because iron and oxygen are often intimately connected in their metabolism, it is not surprising that their levels are coordinately regulated in cells. Such cross-talk is achieved in part by cellular regulatory factors that sense and respond to both iron and oxygen, and it is reinforced by the overlap in the gene targets regulated by each pathway. For instance, binding of IRPs protects TfR mRNA from degradation, and HIF-1α activates TfR gene transcription (36, 37). In addition, in this study, we identified that hypoxia-inducible miR-210 was a key component of this pathway.

As noted above, we have clearly shown that iron homeostasis is micromanaged by miRNAs. Therefore, miRNAs could be essential for maintaining other metal homeostasis in mammals; for example, copper, zinc, and cadmium. In agreement with our observations, the current view on the molecular understanding of miRNA-guided regulation of plant heavy metal adaption was reported (38, 39). Dysregulation of metal homeostasis-related miRNAs may contribute to various diseases including cancers, nephropathy, and autoimmune disease. Further analyses are required on how these miRNAs can be affected by genetic and epigenetic mechanisms in the physiological and pathological microenvironments.

Acknowledgments—We thank Haruhisa Iguchi and Ryou-u Takahashi for participation in discussions and technical advice, Yusuke Yamamoto for participation in helpful discussions, Ayako Inoue, and Keitaro Hagiwara for excellent technical assistance.

REFERENCES

1. Que, L., Jr., and Ho, R. Y. (1996) Dioxygen activation by enzymes with mononuclear nonheme iron active sites. *Chem. Rev.* **96,** 2607–2624
2. Pau, M. Y., Lipscomb, J. D., and Solomon, E. I. (2007) Substrate activation for O_2 reactions by oxidized metal centers in biology. *Proc. Natl. Acad. Sci. U.S.A.* **104,** 18355–18362
3. Hegg, E. L., and Que, L., Jr. (1997) The 2-His-1-carboxylate facial triad: an emerging structural motif in mononuclear nonheme iron(II) enzymes. *Eur. J. Biochem.* **250,** 625–629
4. Stadtman, E. R. (1990) Metal ion-catalyzed oxidation of proteins: biochemical mechanism and biological consequences. *Free Radic. Biol. Med.* **9,** 315–325
5. Clark, S. F. (2009) Iron-deficiency anemia: diagnosis and management. *Curr. Opin. Gastroenterol.* **25,** 122–128
6. Raja, K. B., Duane, P., and Peters, T. J. (1990) Effects of turpentine-induced inflammation on the hypoxic stimulation of intestinal Fe^{3+} absorption in mice. *Int. J. Exp. Pathol.* **71,** 785–789
7. Laftah, A. H., Raja, K. B., Latunde-Dada, G. O., Vergi, T., McKie, A. T., Simpson, R. J., and Peters, T. J. (2005) Effect of altered iron metabolism on markers of haem biosynthesis and intestinal iron absorption in mice. *Ann. Hematol.* **84,** 177–182
8. Peyssonnaux, C., Zinkernagel, A. S., Schuepbach, R. A., Rankin, E., Vaulont, S., Haase, V. H., Nizet, V., and Johnson, R. S. (2007) Regulation of iron homeostasis by the hypoxia-inducible transcription factors (HIFs). *J. Clin. Invest.* **117,** 1926–1932
9. Wang, G. L., Jiang, B. H., Rue, E. A., and Semenza, G. L. (1995) Hypoxia-inducible factor 1 is a basic-helix-loop-helix-PAS heterodimer regulated by cellular O_2 tension. *Proc. Natl. Acad. Sci. U.S.A.* **92,** 5510–5514
10. Wang, G. L., and Semenza, G. L. (1995) Purification and characterization of hypoxia-inducible factor 1. *J. Biol. Chem.* **270,** 1230–1237
11. Campbell, J. A. (1940) Effects of precipitated silica and of iron oxide on the incidence of primary lung tumors in mice. *Br. Med. J.* **2,** 275–280
12. Richardson, D. R., Kalinowski, D. S., Lau, S., Jansson, P. J., and Lovejoy, D. B. (2009) Cancer cell iron metabolism and the development of potent iron chelators as anti-tumor agents. *Biochim. Biophys. Acta* **1790,** 702–717
13. Bartel, D. P. (2004) MicroRNAs: genomics, biogenesis, mechanism, and function. *Cell* **116,** 281–297
14. Stefani, G., and Slack, F. J. (2008) Small noncoding RNAs in animal development. *Nat. Rev. Mol. Cell Biol.* **9,** 219–230
15. Calin, G. A., and Croce, C. M. (2006) MicroRNA signatures in human cancers. *Nat. Rev. Cancer* **6,** 857–866
16. Rasmussen, K. D., Simmini, S., Abreu-Goodger, C., Bartonicek, N., Di Giacomo, M., Bilbao-Cortes, D., Horos, R., Von Lindern, M., Enright, A. J.,

and O'Carroll, D. (2010) The miR-144/451 locus is required for erythroid homeostasis. *J. Exp. Med.* **207,** 1351–1358
17. Kosaka, N., Sugiura, K., Yamamoto, Y., Yoshioka, Y., Miyazaki, H., Komatsu, N., Ochiya, T., and Kato, T. (2008) Identification of erythropoietin-induced microRNAs in haematopoietic cells during erythroid differentiation. *Br. J. Haematol.* **142,** 293–300
18. Camps, C., Buffa, F. M., Colella, S., Moore, J., Sotiriou, C., Sheldon, H., Harris, A. L., Gleadle, J. M., and Ragoussis, J. (2008) HSA-miR-210 is induced by hypoxia and is an independent prognostic factor in breast cancer. *Clin. Cancer Res.* **14,** 1340–1348
19. Friedman, R. C., Farh, K. K., Burge, C. B., and Bartel, D. P. (2009) Most mammalian mRNAs are conserved targets of microRNAs. *Genome Res.* **19,** 92–105
20. Griffiths-Jones, S., Grocock, R. J., van Dongen, S., Bateman, A., and Enright, A. J. (2006) miRBase: microRNA sequences, targets, and gene nomenclature. *Nucleic Acids Res.* **34,** D140–144
21. Wang, X., and El Naqa, I. M. (2008) Prediction of both conserved and nonconserved microRNA targets in animals. *Bioinformatics* **24,** 325–332
22. Huang, X., Ding, L., Bennewith, K. L., Tong, R. T., Welford, S. M., Ang, K. K., Story, M., Le, Q. T., and Giaccia, A. J. (2009) Hypoxia-inducible miR-210 regulates normoxic gene expression involved in tumor initiation. *Mol. Cell* **35,** 856–867
23. Fujita, S., Ito, T., Mizutani, T., Minoguchi, S., Yamamichi, N., Sakurai, K., and Iba, H. (2008) miR-21 gene expression triggered by AP-1 is sustained through a double-negative feedback mechanism. *J. Mol. Biol.* **378,** 492–504
24. Burk, U., Schubert, J., Wellner, U., Schmalhofer, O., Vincan, E., Spaderna, S., and Brabletz, T. (2008) A reciprocal repression between ZEB1 and members of the miR-200 family promotes EMT and invasion in cancer cells. *EMBO Rep.* **9,** 582–589
25. Ye, H., and Rouault, T. A. (2010) Erythropoiesis and iron-sulfur cluster biogenesis. *Adv. Hematol.* **2010,** 10.1155/2010/329394
26. Tong, W. H., and Rouault, T. A. (2006) Functions of mitochondrial ISCU and cytosolic ISCU in mammalian iron-sulfur cluster biogenesis and iron homeostasis. *Cell Metab.* **3,** 199–210
27. Chen, Z., Li, Y., Zhang, H., Huang, P., and Luthra, R. (2010) Hypoxia-regulated microRNA-210 modulates mitochondrial function and decreases ISCU and COX10 expression. *Oncogene* **29,** 4362–4368
28. Favaro, E., Ramachandran, A., McCormick, R., Gee, H., Blancher, C., Crosby, M., Devlin, C., Blick, C., Buffa, F., Li, J. L., Vojnovic, B., Pires das Neves, R., Glazer, P., Iborra, F., Ivan, M., Ragoussis, J., and Harris, A. L. (2010) MicroRNA-210 regulates mitochondrial free radical response to hypoxia and Krebs cycle in cancer cells by targeting iron-sulfur cluster protein ISCU. *PLoS One* **5,** e10345
29. Hentze, M. W., Caughman, S. W., Rouault, T. A., Barriocanal, J. G., Dancis, A., Harford, J. B., and Klausner, R. D. (1987) Identification of the iron-responsive element for the translational regulation of human ferritin mRNA. *Science* **238,** 1570–1573
30. Vaupel, P., Kallinowski, F., and Okunieff, P. (1989) Blood flow, oxygen and nutrient supply, and metabolic microenvironment of human tumors: a review. *Cancer Res.* **49,** 6449–6465
31. Raleigh, J. A., Chou, S. C., Arteel, G. E., and Horsman, M. R. (1999) Comparisons among pimonidazole binding, oxygen electrode measurements, and radiation response in C3H mouse tumors. *Radiat. Res.* **151,** 580–589
32. Chan, S. Y., Zhang, Y. Y., Hemann, C., Mahoney, C. E., Zweier, J. L., and Loscalzo, J. (2009) MicroRNA-210 controls mitochondrial metabolism during hypoxia by repressing the iron-sulfur cluster assembly proteins ISCU1/2. *Cell Metab.* **10,** 273–284
33. O'Donnell, K. A., Yu, D., Zeller, K. I., Kim, J. W., Racke, F., Thomas-Tikhonenko, A., and Dang, C. V. (2006) Activation of transferrin receptor 1 by c-Myc enhances cellular proliferation and tumorigenesis. *Mol. Cell. Biol.* **26,** 2373–2386
34. Chitambar, C. R., Massey, E. J., and Seligman, P. A. (1983) Regulation of transferrin receptor expression on human leukemic cells during proliferation and induction of differentiation: effects of gallium and dimethylsulfoxide. *J. Clin. Invest.* **72,** 1314–1325
35. Neckers, L. M., and Trepel, J. B. (1986) Transferrin receptor expression and the control of cell growth. *Cancer Invest.* **4,** 461–470
36. Lok, C. N., and Ponka, P. (1999) Identification of a hypoxia-response element in the transferrin receptor gene. *J. Biol. Chem.* **274,** 24147–24152
37. Tacchini, L., Bianchi, L., Bernelli-Zazzera, A., and Cairo, G. (1999) Transferrin receptor induction by hypoxia: HIF-1-mediated transcriptional activation and cell-specific post-transcriptional regulation. *J. Biol. Chem.* **274,** 24142–24146
38. Yamasaki, H., Abdel-Ghany, S. E., Cohu, C. M., Kobayashi, Y., Shikanai, T., and Pilon, M. (2007) Regulation of copper homeostasis by microRNA in *Arabidopsis*. *J. Biol. Chem.* **282,** 16369–16378
39. Abdel-Ghany, S. E., and Pilon, M. (2008) MicroRNA-mediated systemic down-regulation of copper protein expression in response to low copper availability in *Arabidopsis*. *J. Biol. Chem.* **283,** 15932–15945

Inhibition of Stabilin-2 elevates circulating hyaluronic acid levels and prevents tumor metastasis

Yoshikazu Hirose[a,1], Eiko Saijou[a,1], Yasuyoshi Sugano[a,1], Fumitaka Takeshita[b], Satoshi Nishimura[c,d], Hidenori Nonaka[a], Yen-Rong Chen[a], Keisuke Sekine[a], Taketomo Kido[a], Takashi Nakamura[e], Shigeaki Kato[e], Toru Kanke[f], Koji Nakamura[f], Ryozo Nagai[c,d,g], Takahiro Ochiya[b], and Atsushi Miyajima[a,2]

[a]Laboratory of Cell Growth and Differentiation and [e]Laboratory of Nuclear Signaling, Institute of Molecular and Cellular Biosciences, University of Tokyo, Tokyo 113-0032, Japan; [b]Division of Molecular and Cellular Medicine, National Cancer Center Research Institute, Tokyo 104-0045, Japan; [c]Department of Cardiovascular Medicine, [d]Translational Systems Biology and Medicine Initiative, and [g]Global Center of Excellence Program, Comprehensive Center of Education and Research for Chemical Biology of the Diseases, University of Tokyo, Tokyo 113-8655, Japan; and [f]LivTech Inc., Kanagawa 216-0001, Japan

Edited by Joan Massagué, Memorial Sloan-Kettering Cancer Center, New York, NY, and approved February 3, 2012 (received for review October 31, 2011)

Hyaluronic acid (HA) has been implicated in the proliferation and metastasis of tumor cells. However, most previous studies were conducted on extracellular matrix or pericellular HA, and the role of circulating HA in vivo has not been studied. HA is rapidly cleared from the bloodstream. The scavenger receptor Stabilin-2 (Stab2) is considered a major clearance receptor for HA. Here we report a dramatic elevation in circulating HA levels in Stab2-deficient mice without any overt phenotype. Surprisingly, the metastasis of B16F10 melanoma cells to the lungs was markedly suppressed in the Stab2-deficient mice, whereas cell proliferation was not affected. Furthermore, administration of an anti-Stab2 antibody in Stab2$^+$ mice elevated serum HA levels and prevented the metastasis of melanoma to the lung, and also suppressed spontaneous metastasis of mammary tumor and human breast tumor cells inoculated in the mammary gland. Administration of the antibody or high-dose HA in mice blocked the lodging of melanoma cells to the lungs. Furthermore, HA at high concentrations inhibited the rolling/tethering of B16 cells to lung endothelial cells. These results suggest that blocking Stab2 function prevents tumor metastasis by elevating circulating HA levels. Stab2 may be a potential target in antitumor therapy.

cancer | hyaluronan | imaging | antibody therapy | sinusoid

Scavenger receptors mediate the endocytosis of metabolic waste products produced under normal and pathological conditions, as well as harmful foreign substances, such as bacterial debris absorbed in the gut. The liver functions as a major filter to eliminate such molecules from the circulation. Liver-specific capillaries known as sinusoids are vital to this function; for example, more than 90% of circulating hyaluronic acid (HA) is cleared by liver sinusoids (1). Sinusoidal walls consist of hepatic sinusoid endothelial cells (HSECs), stellate cells, and liver resident macrophages known as Kupffer cells. HSECs and Kupffer cells express various types of scavenger receptors to fulfill the filter functions. Among those scavenger receptors, Stabilin-1 (Stab1, also known as FEEL-1 and CLEVER-1) and Stabilin-2 (Stab2, also known as FEEL-2 and HARE) are structurally related, exhibiting 55% homology at the protein level, and expressed on HSECs (2).

Stab1 and Stab2 are large type I transmembrane glycoproteins containing four domains with EGF-like repeats, seven fasciclin-1 domains, and an X-link domain (3). Despite these two glycoproteins' structural similarity, the spectrum of their ligands differs significantly. Stab1 is expressed on lymphatic vessels and macrophages as well as HSEC and binds to acetylated low-density lipoprotein (ac-LDL), secreted protein acidic and rich in cysteine, placental lactogen, growth differentiation factor 15, and Gram-positive and Gram-negative bacteria, but not to HA (2, 4–8). It also mediates leukocyte trafficking (9). Stab2 is expressed on the sinusoid endothelium in the liver, spleen, and lymph nodes and has been used as a specific marker for HSECs (10). It binds to and mediates the endocytosis of HA, advanced glycation end products-modified protein, and heparin in addition to ac-LDL, growth differentiation factor 15, and bacteria (2, 4). Stab2 also recognizes membrane phosphatidylserine of apoptotic cells (11). Previous studies found that unlabeled chondroitin sulfate inhibited the uptake of ^{125}-I-HA (12), and that ac-LDL binding to Stab2 was partially competed by heparin and dextran sulfate, but not competed by HA (13). These findings suggest that the HA binding site overlaps with the binding site of chondroitin sulfate but differs from the binding sites of ac-LDL, heparin, and dextran sulfate.

HA is a glycosaminoglycan of the extracellular matrix consisting of tandem repeats of D-glucuronic acid and *N*-acety-D-glucosamine. HA is abundant in the umbilical cord, articular joints, cartilage, and vitreous humor (14). It has been implicated in various physiological functions, including lubrication, water homeostasis, filtering effects, regulation of plasma protein distribution, angiogenesis, wound healing, and chondrogenesis (15). Signal transduction and functions of HA differ depending on molecular size; for example, high molecular weight HA suppresses angiogenesis, whereas HA fragments stimulate angiogenesis (16).

HA interacts with various cell surface receptors, including CD44, Lyve-1, TLRs, RHAMM, and Stab2 (17, 18). CD44, the most extensively characterized of these receptors, is expressed at varying levels in most immune cells and is involved in their rolling and extravasation via HA displayed on endothelial cells (ECs) (19). CD44 is also implicated in tumorigenesis and a marker for cancer stem cells (reviewed in ref. 20). Lyve-1 is structurally related to CD44 and is expressed in lymphatic vessels as well as in HSECs (21). TLR2 and TLR4 bind to HA or a complex of HA and HA-binding protein (18, 22); however, none of the mice deficient for CD44, Lyve-1, or TLRs have been shown to affect circulating HA levels in vivo. Although Stab1 and Stab2 are structurally related scavenger receptors with the HA-binding link domain, only Stab2 binds HA, and thus it has been considered the primary scanvenger receptor for HA (2, 3, 5).

HA, HA synthases (HAS), hyaluronidases, and HA receptors have been implicated in various tumors, including carcinomas, lymphomas, and melanocytic and neuronal tumors (23, 24). Overexpression and knockdown of HAS and hyaluronidases

Author contributions: Y.H., E.S., Y.S., H.N., and A.M. designed research; Y.H., E.S., Y.S., F.T., S.N., Y.-R.C., K.S., T. Kido, T.N., S.K., T. Kanke, K.N., R.N., and T.O. performed research; Y.H., E.S., Y.S., F.T., S.N., and A.M. analyzed data; and Y.H., E.S., and A.M. wrote the paper.

The authors declare no conflict of interest.

This article is a PNAS Direct Submission.

[1]Y.H., E.S., and Y.S. contributed equally to this work.

[2]To whom correspondence should be addressed. E-mail: miyajima@iam.u-tokyo.ac.jp.

This article contains supporting information online at www.pnas.org/lookup/suppl/doi:10.1073/pnas.1117560109/-/DCSupplemental.